FINAL Report: Improved Barrier Properties in Flexible, Plastic Substrates
Contract # W911NF-05-2-0045

Submitted to: Dr. David Morton
U.S. Army Research Lab
2800 Powder Mill Rd
Adelphi, MD 20783-1197
Office (301) 394-1916
FAX (301) 394-0329

Submitted by: Bruce Gnade
Department of Materials Science and Engineering
University of Texas at Dallas
Richardson, TX 75056
Office 972-883-2312
FAX 972-883-2710
E:mail gnade@utdallas.edu

Executive Summary

The influence of a mica thin film barrier on gas permeation properties was investigated. A mica barrier decreases the permeation of helium through polymer substrates by factor of up to 45. Bending these samples causes an increase in the permeation through the sample.

Earlier attempts were made using small size mica flakes to reduce the permeability of flexible polymer films. Aligning these flakes by casting a suspension of flakes in a polymer solution resulted in permeability drop by a factor of 10.[26] Experiments done in this work showed a decrease in the permeability by up to a factor of 45 using a single layer of a thin film of mica (thickness up to 30μm).

A bent PEN-mica sample shows comparatively higher permeation, even when it is shown that mica can be easily bent without damaging the material. A possible answer is that on making a stack, the mica layer is sandwiched between PEN samples using adhesive. The stacking arrangement is not perfect and there are a significant number of air bubbles between the layers, causing uneven stress points on the mica. The misfit strain and the shear stress induced by the forced bending may cause a break in the thin mica film.

More studies on the effects of mechanical stress on making PEN-mica stacks and thus their barrier performance are required. Also, a better way to stack the different layers is required to minimize the number of air bubbles present between the layers, thus increasing the transmittance. It is evident from the results that the permeation through mica films is defect driven. Other barrier layers can be used in conjunction with mica to improve the barrier properties. Mica is a promising candidate as a permeation barrier.

MOTIVATION

1.1 Introduction

Plastics have found a wide acceptance as an alternative construction material for a large number of applications in food packaging, beverage, chemical separation and pharmacy because of their lower cost or lower weight.[1]

Flexible electronic devices are commonly used for applications such as light-emitting diodes, photovoltaic devices or thin-film transistors (TFTs).[2] Flexible plastic substrates are desired in the flat panel display industry[3] where there is a high demand for rugged, lightweight, power efficient flat panel displays. Flexible electronics have the potential to be used in large area electronic devices with much lower cost on an area basis, as compared to conventional silicon technology. One reason flexible electronics have the potential to be inexpensive is because of the ability to apply active layers of the device using low-cost printing techniques that are compatible with high volume "roll-to-roll" manufacturing.[4] A good example of flexible electronics is the organic light emitting diode (OLED). Flexible displays may eventually replace liquid crystal displays (LCDs) that use fragile glass substrates.[5] An example of a personal display would be a device that can be rolled to a small diameter, preferably a radius of less than 10mm.[6] The desired characteristics for a substrate to be usable in organic electronics are thin, lightweight, rugged, flexible, highly transparent, easily processable, low cost, solvent resistant, and impermeable to H_2O and O_2.[3]

- Optical Transparency: Typical display applications require that the substrate exhibit >90% transmittance over the 400-700nm visible range. Optical transparency is an important requirement for the flexible plastic substrate, especially to be used in "down-emitting" device structures where the transparent electrode is the first device layer deposited on the substrate.[4]
- Mechanical Flexibility: One argument in favor of plastics is their potential to be roll-to-roll processed. This demands for mechanical flexibility. A typical metric to quantify mechanical flexibility is the ability to bend the device in a 1-in diameter, 1000 times without a loss of performance.[4]
- Chemical Resistance: The polymer to be used as a substrate should be compatible with the solvents and chemicals used in organic electronic device fabrication steps. A typical list of the materials commonly used for organic electronics fabrication includes methanol, isopropanol, acetone, tetrahydrofuran, n-methylpyrrolidone, ethylacetate, sulfuric acid, glacial acetic acid, hydrogen peroxide, and sodium hydroxide[4].
- Impermeability to H_2O and O_2: Organic materials often show degradation in their electronic properties when exposed to air, water, or ultraviolet light[5]. It has been estimated that the maximum allowable oxygen transmission rate (OTR) is 10^{-8} g/m^2day and the water vapor transmission rate (WVTR) is 10^{-6} g/m^2day (at standard temperature and pressure) to protect these sensitive organic devices.[7] Thus a high level of permeation resistance to H_2O and O_2 is desired in a substrate.

Other leading candidates for flexible substrate materials are ultra-thin glass and metal foils, which provide effective permeation resistance and thus eliminate the need for further barrier layers.[8] OLEDs built on glass substrates have been shown to have lifetimes of tens of thousands of hours.[9] However, glass substrates do not allow exploitation of the intrinsic flexibility of polymers.

Though flexible substrates are superior to conventional materials in terms of weight, flexibility, ruggedness and the ability to be produced using roll-to-roll manufacturing, etc; they are not widely used because of facile permeation of atmospheric gases such as O_2 and H_2O. Exposure of the organic-cathode interface in an OLED to atmospheric oxygen or water leads to oxidation and de-lamination of the metal cathode and chemical reactions within the organic

layers,[9] reducing the lifetime of the device. Polymer substrates do not offer the same barrier performance as glass or metal foil. Therefore, they require an external thin-film barrier on both the bottom and top surfaces of the device for acceptable lifetimes. A major factor for extending the lifetime of atmospherically sensitive devices is a barrier coating that will provide adequate protection from oxygen and moisture permeation.[7]

For commercially available polymers, such as Polylmide (PI), PolyTetraFlouro Ethylene (PTFE), PolyEthylene Terephthalate (PET) and PolyEthylene Naphthalate(PEN), the permeation rates are typically $\geq 1x10^{-3} g/m^2 day$ for oxygen and $\geq 1 g/m^2 day$ for water depending on the thickness of the polymer.[10] WVTR for a 25μm thick PEN and PET is 6.7 $g/m^2 day$[11] and 21.3 $g/m^2 day$[11] and their oxygen transmission rate is $2.7x10^{-2}$ $g/m^2 day$[11] and $7.15x10^{-2}$ $g/m^2 day$[11]. The required level of hermeticity is beyond the capability of any known plastic film, and therefore plastic substrates need to be coupled with a barrier coating to provide the required hermeticity and meet the other requirements as desired in a substrate.

The best way to achieve a barrier film would be to make films of highly impermeable polymers, though the polymers available are not impermeable to the degree of protection required.[12] PEN and PET are the most widely used polymers as substrates for flexible devices.[11] Another way will be to introduce selective reactive groups within the film that react with and neutralize penetrant molecule such as oxygen, acid or water.[13] The drawback for this technique is that the barrier is rendered ineffective once these reactive groups are exhausted.[13] Another way to make a good barrier film is to add impermeable flakes to the polymer that cause the penetrant molecule to follow a tortuous path through a maze of flakes[14] – a concept used in this study.

The ideal material to be used in the flexible electronic industry would be one that combines the barrier, thermal and scratch resistant properties of glass with the flexibility, toughness and easy-processability of plastic.[3]

This project supported in part the MS thesis of Namrata Bansal. As part of this project, the University of Texas at Dallas also provided support so that we could build an ultra-high vacuum permeability measurement system, which provides state-of-the-art permeation measurement capability.

1.2 Goals

The quality and type of barrier used on the polymer depends on the end-use requirements. For instance, organic light emitting diodes require very high, glass-like barrier performance to achieve isolation of atmospherically sensitive chemicals used in OLEDs from O_2 and H_2O.[7,8,15] Metal oxide barrier films, such as aluminum oxide have been successfully employed by the food packaging industry, however the surface roughness and intrinsic defects, allowed in food packaging industry, prevent the same technique from being utilized as substrates for OLEDs.[16]

The research for this project was done with the requirements for a flexible OLED barrier in mind. The main requirements in a barrier needed for OLEDs can be summarized as:

- Surfaces of plastic substrates are observed to have spikes up to 150nm,[3] while the typical thickness of organic layers to fabricate the electronic device is 100 to 200nm. Any non-uniformities in the surface of this order will lead to deleterious effects on the device performance, and early device degradation.[8] Barrier structures should provide a smooth surface for further processing.
- The majority of permeation through a barrier film is though pinhole defects, also known as defect-driven permeation.[2] The remaining permeation is a result of surface roughness and the low density of the film.[2] To eliminate this effect, the barrier film should have either a high density or the ability to be used in multilayer structures.

- The barrier should be stable and must exhibit good adhesion to the device through the lifetime of the device itself.[3]
- When deposited on the top of a device as an encapsulation layer, the barrier deposition process should not affect the device performance;[8] the deposition process should be at a low temperature that can be tolerated by the polymer used in the device, and the active components of the OLED should not come in contact with any chemical during the barrier deposition process that could degrade the device performance.

1.3 Literature Review: Barrier Films

Over the last few years, there has been significant development in the area of barrier technology for flexible electronics. While there are a large number of barrier solutions being worked upon, the innovations fall into these main categories:[1] a) thin, transparent vacuum-deposited coatings, b) new barrier polymers, c) organic barrier coatings and d) Inorganic-organic hybrid coatings. This section is a review of the different approaches being developed towards a viable barrier technology.

1.3.1 Barrier Polymers

Research is being done on polymers with intrinsic high permeation resistance as compared to the commonly used polymers such as PEN or PET. The oxygen permeation rate for 25μm thick PEN and PET is $2.73x10^{-2}$ g/m^2/day[11] and $7.15x10^{-2}$ g/m^2/day[11]. Ticona has developed a liquid crystalline polymer (LCP), which has an oxygen permeability rate 50-100 times lower than PET.[1] Though the LCPs have both low diffusivity and exceptionally low solubility for a gas molecule, they are not widely used because of their high cost and translucency in even thin layers.[1,17] The high cost of LCPs is due to the high cost of the monomers used for their synthesis.[17] Thus other attempts are being made to attain the barrier characteristics of the LCPs at a low cost by blending these monomers in a small amount with conventional, inexpensive polymers such as PET.[17]

1.3.2 Inorganic Barrier Coatings

Thin-film permeation barriers have been formed from aluminum, aluminum oxide and silicon oxide.[2,18] In bulk, these films are impermeable to oxygen and water. SiO_x thin-films are generally deposited on polymers by physical vapor deposition (PVD) or plasma-enhanced chemical vapor deposition (PECVD).[1] While these SiO_x films are thin and transparent, they provide only two to three orders of magnitude improvement in oxygen and water permeation rates.[2] Also, they are brittle and have a limited flexibility and crack resistance.[1,19] Iwamori et. al. studied the oxygen transmission rates for thin film SiO_x deposited on 25μm thick PET by sputtering.[18] The deposited SiO_x layers varied in thickness from 10nm to 40nm. The increase in thickness of the film beyond 25nm had a negligible effect, and the lowest OTR value of the SiO_x film was $8.6x10^{-4}$ g/m^{2}day.[18]

Henry et. al. studied the oxygen and water vapor transmission properties of different aluminum oxide layers deposited by electron-beam evaporation and reactive magnetron sputtering.[20] AlO_x layers of thickness from 1nm to 17nm were deposited onto untreated 12μm PET substrates using either technique and the oxygen and water vapor transmission rates were measured using a Mocon instrument. The oxygen permeation rate through the bare PET (0.23 g/m^2/day) was reduced to $6.11x10^{-3}$ g/m^2/day[20] through PET with a 17nm AlO_x layer deposited by e-beam evaporation. A similar decrease in the permeation of water vapor was shown, from 53.1 to 1.7 g/m^2/day.[20] In another set of experiments, Dinelli et. al. deposited thin AlO_x films by sputtering a few monolayers of aluminum, which was converted to oxide by application of an oxygen plasma.[21] The best results achieved, with an AlO_x film of thickness 30nm on a 12μm

thick PET substrate, were an oxygen transmission rate of $2.08x10^{-3}$ g/m^{2}day[21] and a water vapor transmission rate of 0.42g/m^{2}day[21]. Ohya, et.al. deposited a double layer coating by simultaneously evaporating Al_2O_3 and SiO_2 by one e-beam-gun.[22] For a thickness of 50nm, the oxygen transmission rate achieved was $3.25x10^{-3}$ g/m^{2}day.[22]

Pinholes in oxide films related to high surface roughness of commercially available polymer substrates, or handling of the substrate after deposition of the oxide layer, limits its effectiveness as a barrier[23]. A permeability rate $<10^{-2}$ g/m^{2}day for water vapor is difficult to achieve.[9]

Recent studies using an atomic layer deposition (ALD) process showed films deposited by this process can be smooth, conformal, and pinhole-free. High quality Al_2O_3 films were deposited by ALD at temperatures as low as 33°C by Groner, et.al.[10] Al_2O_3 ALD films with thicknesses of 10nm deposited on PEN exhibited an oxygen transmission rate $< 6.5 \times 10^{-6}$ g/m^{2}day.[10] Also, the water vapor transmission rate dropped from ~1g/m^{2}day for the uncoated polymer film to ~ $2x\ 10^{-3}$ g/m^{2}day for the Al_2O_3 coated substrate.[10]

1.3.3 Organic Barrier Coatings

Hydrocarbon (HC) films can also be deposited on polymers by PECVD. Amorphous carbon (a-C) and hydrogenated amorphous carbon (a-C:H) have superior properties to SiO_x films for wear and mechanical hardness[1,19]. Oxygen permeation through hydrocarbon films was studied by Moser et. al.[19] Thin hydrocarbon barrier layers, deposited by either dc magnetron sputtering or PECVD onto PET substrates of thickness 12μm, were amorphous with their stoichiometry varying between $C_1H_{0.2}$ and $C_1H_{0.5}$.[19] The benefit of such a film is the intrinsic flexibility and an increase in oxygen permeation resistance by up to 120.[19] Results show that the oxygen permeation rate, measured using a MOCON OX-TRAN 2/20 instrument, decreased from 0.16 g/m^{2}day-bar for bare PET to $1.4x10^{-3}$ g/m^{2}day-bar for a 76nm thick a-C:H film with an optical transmission >70%.[19]

1.3.4 Hybrid Coatings

There is considerable work being done on polymer-barrier multi- layers to achieve ultra-high barrier performance. Polymer multi-layers (PML) with the configuration polymer/barrier/polymer were studied by Affinito et. al.[23] This process entails deposition of polymer films and oxide layers on a substrate to get a transparent barrier coating. Al_2O_3 was deposited by PECVD, which was compatible with the PML process.[23] For a deposition of 1μm PML – 25.5 nm Al_2O_3 – 0.24μm PML coatings,[23] deposited on 50μm thick polyester, the oxygen and water vapor transmission were found to be $2.015x10^{-5}$ g/m^{2}day and $1.55x10^{-2}$ g/m^{2}day.[23] This enhancement in permeation barrier properties is attributed to the polymer layers deposited before and after oxide deposition. The first polymer layer provides a smooth surface for oxide deposition by eliminating the substrate defects, and thus the deposited oxide layer has few pinholes as compared to the number of pinholes in an oxide layer deposited directly on the surface. The second polymer layer deposited on the oxide layer prevents scratching of the barrier layer.

Another hybrid organic-inorganic multilayer barrier coating was studied by Weaver et. al.[9] This composite barrier consisted of alternating layers of polyacrylate films and 10-30nm thick Al_2O_3 films, that collectively were transparent and thin enough to maintain flexibility.[4,9] These alternate organic polymer layers decouple the pinhole defects in the inorganic oxide layers, increasing the tortuosity of diffusion path, thus effectively reducing the permeation rate to $<1.3x10^{-5}$ g/m^{2}day for O_2 and $<2x10^{-6}$ g/m^{2}day for water vapor.[9]

1.4 Motivation behind studying mica as a prospective barrier material

Mica has many attractive features for use as a barrier film including; a) the ability to be cleaved in thin, resilient films that are colorless and transparent, b) high tensile strength, c) inertness to

most chemical compounds and d) high thermal stability. Mica can be easily hand cut or split into thin films along its cleavage plane. [24]

In this work, these features of mica are exploited to develop a barrier structure, where impermeable plates of mica are aligned with the polymer substrate. The motivation for introducing these platelets of ultra-thin mica films is the idea that the permeability through the integrated structure is reduced because the aligned plates increase the path length the intruding molecule has to traverse to pass through the film.[25] Because of the presence of these non-permeable platelets, the penetrating molecule will have to follow a more tortuous path, parallel to the surface of the polymer. Randomly shaped and randomly distributed non-permeable flakes will impede the path of the permeating molecule as it tries to diffuse around the nearest boundary until it encounters a gap along the next random flake.[14,20] This is not a novel idea and has been employed in several applications such as food packaging materials, paints, etc.;[20] where the diffusion is retarded by the tortuous path around the flakes and most of the diffusion occurs around the nearest boundary.[14] Each point on the edge of the impermeable flake represents a possible conduit for diffusion.[2]

These non-permeable platelets, which have been used previously, having a small size, do not increase the tortuous path to the desired extent. Experiments have been done to reduce permeability by aligning mineral flakes, the largest dimension of which was one micron[26]. Thus, in this work, an attempt has been made to work with large sheets.

The idea is to integrate polymer substrate materials with large platelets of mica to improve the permeation barrier properties. The model is a polymer having a few layers of impermeable thin sheets of mica surrounding it. Permeation through such barrier polymer/ membranes might occur through a few defects or pores present in the mica films.

Figure 1.1 shows an example of such a combination of mica and a commonly used polymer substrate PEN (Poly Ethylene Naphthalate) to reduce the permeability of O_2 and H_2O. Mica layers having thickness of 5μm and an area of approximately 50cm^2 have been employed in the formation of the barrier film.

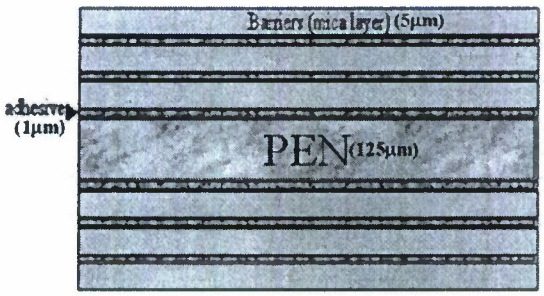

Figure 1.1. Generic structure for the proposed barrier-polymer substrate (5"x5").

A multilayered structure is beneficial, as the mismatch of positions of defects in the film increases the tortuous path of the diffusing molecule, decreasing the permeation rate. The 'decoupling' of defects increases the likelihood of having good barrier properties. [2]

The issues discussed in this work are:

1. Fabrication of mica thin films.
2. Formation of the PEN-mica stacks (as shown in Figure 1).
3. Optical transparency of the mica-polymer substrates.
4. Effect of flexing on the permeation resistance of mica-polymer substrate.

The overall objective of this research is to substantially decrease O_2 and H_2O permeation rates, while maintaining good mechanical, optical and chemical resistance properties.

LITERATURE REVIEW: MICA

2.1 Mica Overview

Mica is a generalized term applied to a group of aluminosilicate minerals having a sheet or plate like structure with highly perfect basal cleavage[27]. Chemically, micas are stable, complex hydrous silicates of aluminum, containing traces of several other elements. Mica crystals have a unique property of being able to be split into films of very small thickness.[24]

Mica usage dates back to prehistoric times, the earliest ones were found in cave paintings and sculptures as coloring agents[27]. Mica is found in a wide range of products from household accessories to electric, thermal, heat and chemical barriers used in various applications[28]. Mica is also used in blow-molded, high-density polyethylene as an agent to enhance the strength, rigidity and temperature resistance.[28] Polymers coated with mica flakes are being studied in different research to provide a barrier against different gases or other compounds.[14]

The generalized formula for mica is $AB_{2-3}(T,Si)_4O_{10}(O,F,OH)_2$[29]. The basic structural feature for mica consists of two negatively charged identical tetrahedral sheets, usually of silica: SiO_4[30], sandwiching a sheet of octahedral shaped coordinated cations. A quarter of these tetrahedral layers have a formula of T_2O_5[29], where the T ion is usually aluminum, but can also be Be, B and/or Fe^{3+}. The vertices of these tetrahedrons point towards each other, as shown in figure 2.1.[30] These vertices are then cross-linked with the interlayer of cations on the octahedral sites, B. The sheet of cations is normally made up of Mg, Al, Fe^{2+}, and Fe^{3+}, but other medium sized cations such as Li, Ti, V, Cr, Mn, Co, Ni, Cu and Zn also occur, in some species.[29] This cross-linked double layer silicate structure is bound firmly and has a slight negative charge.[30] This negative charge is compensated by an interlayer of large cations, A. These cations are usually K or Na in the true micas, and Ca or Ba in brittle micas.[31,29] The cross-linked double layer silicate structure layer is referred to as one 'mica layer' and represents the minimum thickness at which the mica layer can be cleaved.[30]

Mica can be divided in two major divisions based on the interlayer ion charge per formula unit. Flexible micas have singularly charged ions. Doubly charged ions compensate for a major part of the negative charge in brittle micas.[31] Both forms of mica have inclusions, precipitates, and dislocations inherent in the mineralogical structure.[32]

In this work we used flourophlogopite, $KMg_3(Si_3Al)O_{10}F_2$, a flexible mica, in an attempt to get a barrier which fulfills the requirements needed for a 10,000hr operating lifetime for an OLED.

2.2 Mica Properties

Phlogopite mica has a layered structure as described in section 2.1, in which a quarter of the tetrahedra have aluminum at their center and the rest have silicon at the center,[32] as shown in figure 2.1. Since aluminum has a valence charge of 3^+ compared to the 4^+ charge of silicon, there is an imbalance of charge, and a compensation of charge is required to maintain the electrical neutrality. For each Al^{3+}, a positive charge outside of the three-layer 2:1 sandwich is required to balance this charge deficit. The extra charge is provided by a layer of large cations, usually potassium or sodium ions (K^+).[32,30] Each of the potassium ions in this interlayer is shared among 12 oxygen atoms and the electrostatic force between the potassium ion and the oxygen atoms is much less than between a single potassium-oxygen pair.[30,32] This potassium-aluminum-silicon interface is weak.[32] Combined with the high strength of the bonding system within the alumino-silicate and anionic structural layers, the weaker interface provides for easy

cleavage of the micas at this interface.[32] The weak cleavage interface allows us to separate the bulk mica into very thin layers to be used as a barrier layer.

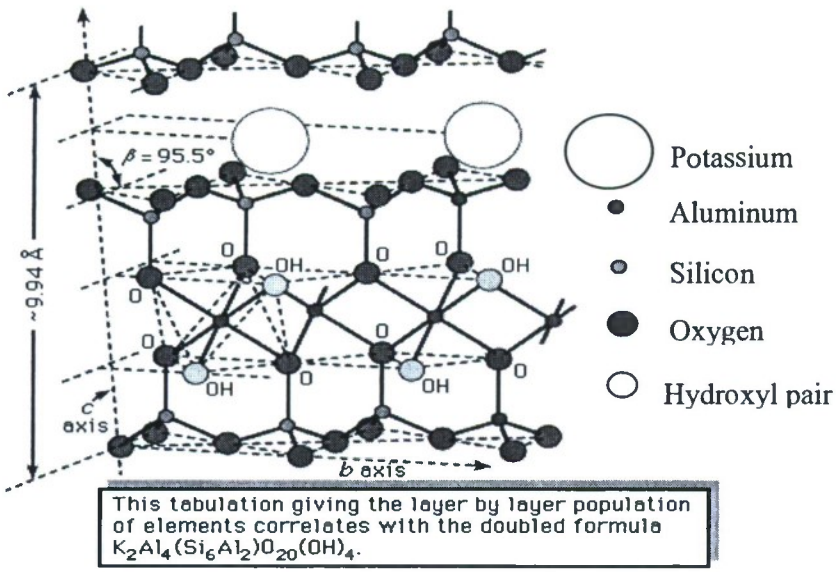

Figure 2.1. A simplified structure of mica.[33] [Reproduced with permission from © 1983, W. H. Freeman and Co.]

These cleaved mica sheets can be colorless and transparent, while maintaining a robust strength through the other two axes. These sheets of mica are relatively soft, with a hardness of 2.3-3.0[32] on the Moh scale. The sheets are flexible and have a high tensile strength of 100 MPa.[32] Phlogopite mica is softer than other micas, resulting in ease of production of flakes or films.

Micas are stable and virtually inert to reaction with water, solvents, oils, alkalies and acids (with the exceptions of hydrofluoric acid and concentrated sulfuric acid).[32] This fulfills another barrier requirement, the ability to withstand different solvents used during OLED fabrication. Micas have low thermal conductivity, typically in the range of 0.04-0.5 $Wm^{-1}K^{-1}$, excellent thermal stability and can resist temperatures as high as 600°C to 900°C.[32]

A long lifetime for a barrier includes maintaining good adhesion to the display surface, a property exhibited by cleaved mica. By cleaving mica along the potassium interface, the potassium layer divides itself equally between the two surfaces, leaving a positive charge on either surface.[32] If an organic adhesive, such as an epoxy resin is used, the ester bond structure with a partial negative dipole interacts strongly with the positive potassium ion generating a strong adhesive force between the two materials.[32]

2.3 Mica as a Barrier

Traditionally thin-film permeation barriers have been formed from Al or Si, Al –oxides. While in bulk form these materials are effectively impermeable, in thin-film single barrier layers, they provide a reduction in permeation rate by 10-100x.[2] This is due to permeation of atmospheric

gases through defects or nano-scale pores or pinholes.[2] This is even more exacerbated with the high surface roughness of commercially available plastic substrates such as polyethylene terephthalate (PET), polycarbonate (PC) and cyclic olefin copolymer (COC).[2] According to United States Display Consortium, plastic substrates should have a surface roughness <2nm rms.[34] While PET and PC can have a surface roughness of 1.4nm rms[35] and 2.7nm rms[35], respectively, plastics such as COC have a surface roughness as high as 131nm,[36] and is unable to achieve the required permeation resistance using inorganic layers.[9] Mica is smooth and can be used to cover these inconsistencies.

Table 2.1. Characteristics of mica[29,30,33,32]

Characteristics		Units
Chemical Information		
Chemical structural formula	$KMg_3(Si_3Al)O_{10}F_2$	
Acid Reaction	Concentrated Sulphuric	
Mechanical Properties		
Hardness	2.3-3.0	Moh
Tensile strength	100	MPa
Shear strength	100-130	MPa
Modulus of elasticity	1.4-2.1	Kgf/cm^2
Thermal Properties		
Thermal conductivity	0.04-0.5	$Wm^{-1}K^{-1}$
Maximum operating temperature	800-900	°C
Calcining temperature	900-1000	°C

Mica has the potential to fulfill the requirements of a barrier as listed in section 1.2. The mechanical stability and permeation barrier properties of mica are investigated in this research. Other requirements such as optical transparency, UV stability, dimensional stability, and cost effectiveness are also satisfied with mica as a barrier. Mica possesses a combination of chemical, physical, electrical, thermal and mechanical properties as listed in Table 2.1.

2.3.1 Permeability dependence on the size of the silicate layer

The prospect of increased permeation resistance of a polymer embedded with mica flakes makes it an attractive option for high performance barriers. However to gain a substantial increase in the tortuous path, and hence an enhancement in the barrier performance, it is required that the fillers or flakes be aligned parallel to the film's surface and perpendicular to the direction of diffusion, as shown in figure 2.2.[25,26]

Earlier attempts in making composite films of mica in PET included adding mica to an extruder through which the polymer was being forced.[14] A reduction in the permeation through the polymer by a factor of 10 was seen by using mica flakes up to the size whose largest dimension was about 1μm with an aspect ratio of 30.[26] Mica flakes were aligned in a PVA film by Cussler et. al. [37] With a mica volume fraction of about 0.2, permeability reduction by a factor of 5 was achieved.[37] In another attempt, mica was used to reduce the permeation of carbon

dioxide through a polymer. It was found that the membranes containing mica flakes had a much lower permeability than membranes without mica flakes.[38] Ward et. al. also used mica flakes to reduce the permeation of carbon dioxide through PET,[39] with PET films filled with 15 and 30% mica showing a permeation of carbon dioxide 4-8 times lower than pure PET.[39]

Because the diffusing molecule cannot permeate the silicate platelets, it must go around them, thus leading to a tortuous path. The non-permeable platelets used in previous attempts had a small size, and thus a lower impact on the increase in tortuous path, as shown in figure 2.2a. The motivation for incorporating high aspect ratio flat sheets of mica is that the tortuosity path should increase greatly, as shown in figure 2.2b.

a)

b)

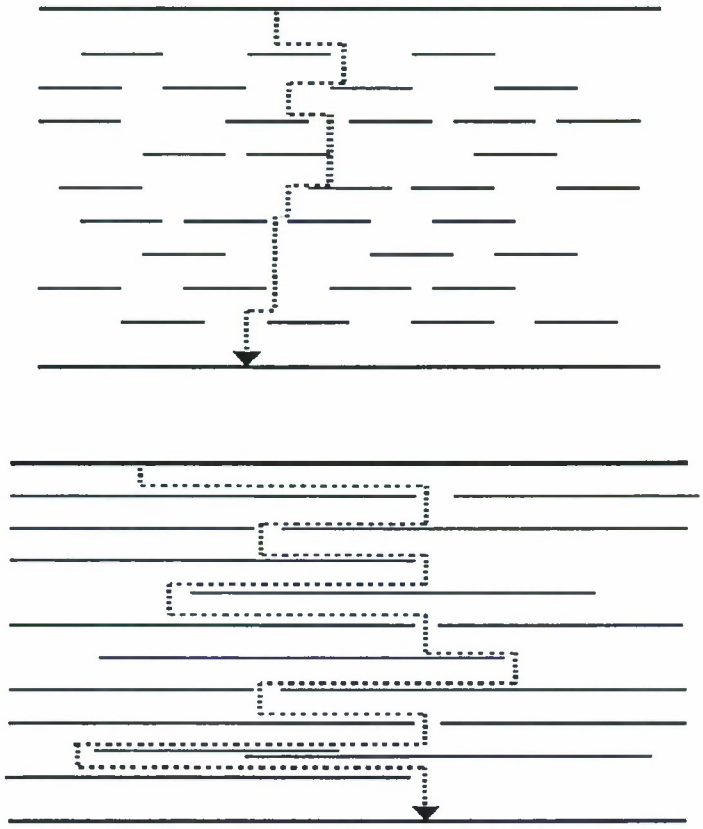

Figure 2.2. Effect of the platelet size on tortuosity, the arrow represents the path of the penetrant.

The tortuosity factor (τ), defined as the ratio of the actual distance (d_{eff}) traveled by a diffusing molecule to the shortest distance (d) it would have traveled in the absence of the layered silicate structures, is given as:[40,41,42]

$$\tau = \frac{d_{eff}}{d} = 1 + \frac{L}{2t_s}\phi_s \qquad (2.1)$$

where, L is the length, t_s is the thickness and ϕ_s is the volume fraction of the silicate layers. The effect of tortuosity on the permeability is expressed as:[40-43]

$$\frac{P_s}{P_p} = \frac{1-\phi_s}{\tau} \qquad (2.2)$$

where, P_s and P_p represent the permeabilities of polymer-silicate structure and pure polymer, respectively. Keeping the thickness, t_s, of the silicate platelets constant, the effect of sheet size on the tortuosity factor and relative permeability is shown in figure 2.3 and figure 2.4.

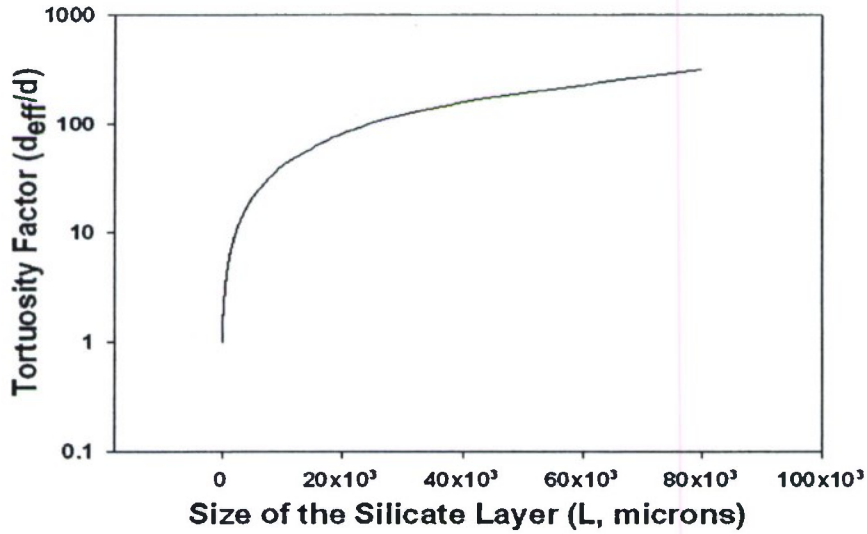

Figure 2.3. Dependence of the tortuosity factor on the sheet length of the silicate layer.

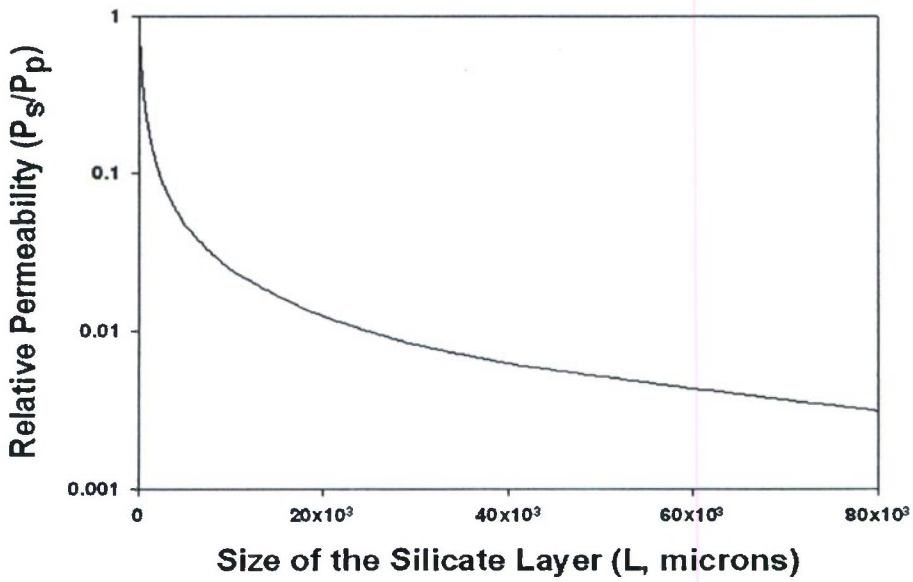

Figure 2.4. Dependence of the relative permeability on the sheet length of the silicate layer.

2.3.2 Diffusion through the Silicate Layers

For polymer substrates, as shown in figure 2.2-b, the dominant transport mode is diffusion and is a function of the concentration gradient. Diffusion is a process induced by the random thermal motion (Brownian motion) of molecules and ions.[44] When diffusion takes place through such a barrier-polymer substrate, the diffusing molecules have to go around these barriers, positioned parallel to the film surface. This is likely to reduce the diffusivity through the substrate. Under steady state conditions,[45] the diffusive flux, F, can be given in accordance with the Fick's first Law as:[44,45]

$$F = -D_{eff}\frac{dC}{dx} \tag{2.3}$$

where, C is the molecular concentration on the high pressure side of the sample (no. of atoms per unit volume), x is the distance along the shortest diffusion path (perpendicular to the surface of the polymer). D_{eff} is the effective diffusion coefficient [L^2T^{-1}], which for this polymer substrate can be defined as:[44,45,46,47]

$$D_{eff} = D_o\frac{\varepsilon_{eff}}{\tau} \tag{2.4}$$

where, D_o is the diffusion coefficient of the bare polymer. ε_{eff} is the vacancy factor, which accounts for the reduced cross-sectional area available for diffusion in the barrier-polymer substrate. Relative diffusivity can be expressed as:

$$\frac{D_{eff}}{D_o} = \frac{\varepsilon_{eff}}{\tau} \tag{2.5}$$

It is noteworthy that the percentage reduction in the diffusion coefficient through the polymer-barrier substrate is because of the increase in the diffusion path and independent of the nature of the diffusing molecule.

2.3.3 Effect of solubility on the lag time

An understanding of gas solubility is important because this behavior is critical to the use of silicate layers (mica) as permeability barriers, since steady state barrier properties and analysis are not adequate. To model permeation through a single barrier layer of thickness, t_s, a concentration profile for the permeant is assumed to be a function of distance and time, C(x,t). Further, it is also assumed that the concentration or pressure on both sides is maintained, which is high pressure at one end and vacuum at the other. The diffusion flux is obtained from Fick's first law and Fick's second law gives the concentration gradient solution for a non-condensable gas.[48] As the thickness of the barrier layer increases, the total mass transmitted through the barrier, Q, in the steady state regime, is given as:[48,49]

$$Q(t\to\infty) = \frac{D_oC}{t_s}\left(t - \frac{t_s^2}{6D_o}\right) \tag{2.6}$$

Where, t is time, t_s is the thickness of the silicate barrier layer, $\frac{t_s^2}{6D_o}$ denotes the offset or the lag time in achieving the steady state[48].

From the diffusivity-tortuosity factor relation, it can be inferred that the percentage diffusivity reduction achieved would be identical for any molecule or ion diffusing through the substrate, assuming that no significant adsorption is occurring on the surface of the silicate layers. For example, the percentage diffusivity reduction observed would be far less than theoretically calculated for diffusion of water molecules. Since the silicate layer is hydrophilic,[32,45] the water molecules entering the polymer surface will saturate these silicate layers before diffusing further into the barrier-polymer substrate. Thus, when the diffusing molecule is strongly attracted to the barrier surface, sorption effects also need to be considered to indicate the maximum possible reduction in diffusivity.[45] In such a case, the gas solubility effect could be seen as an additional reduction in the diffusivity of the gas. From the diffusivity-lag time inverse relation, it is evident that a fall in diffusivity of the gas will result in an increase in the lag-time to reach the saturation steady state regime. Thus, an increase in the solubility of the gas in the polymer-barrier substrate reflects an increase in the lag-time to reach the steady state regime.[49]

EXPERIMENTAL

3.1 Equipment

Permeation is the penetration or transfer of a substance (the permeate) through a solid.[50] The permeate always migrates towards the area of low concentration in three main steps: absorption at the interface of the solid with the high concentration gradient, diffusion through the solid through pores or molecular gaps, and finally desorption as the adsorbate leaves the solid.[51,52] The permeation rate is dependent on the diffusivity of the gas through the solid and the solubility of the gas in the solid, as detailed in section 2.3.2.

There are two basic methods for measuring permeability using vacuum on one, or both sides of the film: isostatic and quasi-isostatic. The quasi-isostatic method is an accumulation procedure[53] and uses gas analysis for quantifying the amount of gas that diffuses through the film. In this method, a constant penetrant concentration is maintained on the feed side, thus allowing for the accumulation of the penetrant on the lower concentration side of the film.[54] For isostatic methods, the test system allows for a continuous collection of permeation data and the penetrant concentration is monitored as a function of time. [53]

To determine the upper limit on acceptable moisture permeation for an operating OLED, a calculation is made based on the assumption that oxidation of the low work function metal cathode in the organic device limits the operating lifetime.[3] Assuming a Mg cathode in the OLED, having a thickness 50nm, density 1.74g/cm^3 and molar mass of 24g, it is estimated that such cathode is completely oxidized by ~6.4x10^{-6}g of water.[3] For a lifetime of a year, maximum leak rate obtained is 1.5x10^{-4} g/m^{2}day.[3] Similarly, permeation barrier requirement for an OLED operating lifetime of 10,000 hrs is a maximum permeation rate of 10^{-6} g/m^2/day for water vapor,[3,7] which exceeds the minimum sensitivity of traditional permeation rate measurement techniques by over 100x.[2] For example, the commercially available MOCON Detection instrument employs a diffusion cell, where one side of the sample is purged of oxygen via an oxygen free gas. The oxygen gas is monitored via a coulometric sensor. The coulometric sensor utilizes a gas flow path which has a predetermined section constructed with oxygen-permeable tubing, wherein a portion of the oxygen flowing through the gas flow path will permeate into the sensor to generate an electric current flow indicative of the permeating oxygen level.[55] When the cell has no oxygen left, the feed side is filled with 99.9% oxygen gas and the diffusion of the gas is then measured as a function of time.[56] This MOCON detection instrument has a limit of 5x10^{-3} g/m^2/day at 25°C,[16] which is ~500x higher than the required detection limit of 1x10^{-6} g/m^2/day.

New approaches have to be applied to determine the permeability of thin-film barriers. The most widely used approach is the calcium test,[57] which monitors the change in transparency of calcium as an indication of permeation. A second approach is the use of an ultra-high vacuum residual gas analyzer to monitor the permeation of various atmospheric gases.[56]

The calcium test method, as described by Nisato et. al.,[57] is based on the corrosion of thin calcium films in the presence of atmospheric oxygen and water vapor. A Ca film is deposited on the substrate whose permeability is to be tested and is then hermetically sealed with a glass lid, using adhesive. The calcium layer is highly reflective initially, but changes into an increasingly transparent layer of calcium salt as it reacts with oxygen and water.[9,57] Transmission rates in the range of 10^{-1} to 10^{-5} g/m^2/day[57] have been determined using this method. An improvement in the calcium test method, as given by Paetzold[58] et. al., measures the electrical resistance of the calcium film, based on the assumption that the oxidized calcium salts are insulators and the corrosion of the calcium strip is homogenous. The calcium test method requires hermetic glues to seal the sample and the use of glass-to-glass control is critical.[57] The sensitivity of this technique is about 5x10^{-5} g/m^2/day.[58]

Though the sensitivity of the calcium test method is much better than that of the other commercially available permeation detection instruments, it is still less than the required sensitivity. While the calcium test provides a convenient way to compare performance of different substrates, it is a comparative test and its quantification is challenging.[57] Thus, the permeation coefficients for the transport of Helium through bare and mica-covered PEN samples were measured with the High Sensitivity Gas Permeability Measurement System.[56] The sensitivity for this instrument for O_2 is approximately $1x10^{-6}$ g/m^2/day.

3.1.1 Schematic Design of the UHV Permeation Measurement System

The experimental setup for the UHV permeation measurement system is shown in Figure 3.1. The basic technique employed in the system is based on creation of a concentration gradient of the gas under analysis across the mounted sample. This concentration gradient drives the permeation of the gas from high concentration to low concentration and the permeation is monitored over time.

The sample holder marks the division between the two sides of the vacuum system: a high-pressure or low-vacuum side and an ultra high vacuum (UHV) side.

The UHV side, on the left hand side of Figure 3.1, is built around a $4^{1/2}$ in. conflat flange, six-way cross. It is equipped with a 125 l/s Varian StarCell ion pump[59] and a titanium sublimation pump. The UHV side is pumped by a 240 l/s turbo molecular pump to reach a base pressure of 10^{-8} Torr. The ion pump and the sublimation pump are used to achieve the required total base pressure, which is approximately 10^{-10} Torr. The UHV side is connected to the N_2 vent line via vent valve, U_5. The overall pressure of the UHV side is monitored with a ThO_2/Ir ion gauge. The partial pressures of the gases being monitored are measured with a residual gas analyzer quadrupole mass spectrometer, fitted with an electron multiplier for increased sensitivity.[60] The UHV side of the system also has a National Institute of Standards and Technology (NIST) traceable calibrated helium leak for the purpose of calibration of the system.[56] For the purpose of calibrating the system for gases other than He, a three-positioned/apertured gate valve, FU, separating the UHV chamber and the high-pressure chamber, is positioned to allow the introduction of small orifices required during the calibration procedure.

The high-pressure side, the right hand side of Figure 3.1, is built around a $4^{1/2}$ in. conflat flange, six-way cross. The right-most flange of the cross has a view-port attached, which allows viewing of the sample while the experiment is being performed. The high vacuum side is pumped with a 180 l/s turbo-molecular pump attached to the cross via a pneumatic gate valve, F_1. Valve F_1 isolates the turbo pump when the test gas is at high pressure in the chamber. The sample can be isolated from the high-pressure side with the gate valve F_2, and the right angle bypass valve, F_3. The base pressure is measured with a ThO_2/Ir ion gauge attached to one of the flanges of the six-way cross. When gas is bled into the chamber, the gas pressure is monitored with a thermocouple gauge (10^{-3}-1 Torr) and a capacitance manometer (1-10^3 Torr). The capacitance manometer is used to monitor the pressure on the feed side during measurements, because it is absolutely calibrated in the range of 1-1000 Torr. While under vacuum at a pressure at or below the maximum zeroing pressure for the capacitance manometer, zero adjustment is made. The system is connected to the N_2 vent line through F_7.

Helium and other analyzing gases are introduced into the high-pressure side of the system through a sapphire leak valve, F_5. To prevent leakage into the system through this valve, another valve, F_4 connects the sapphire leak valve to the gas manifold valves, F_6.

3.1.2 Calibration of the System

The change in the partial pressure of the analyzing gas on the UHV side is monitored with a residual gas analyzer. The purpose of calibrating the system is to determine the correlation

between the partial pressure of the analysis gas measured with the RGA to the flow rate of gas atoms through the sample film from the feed side to the UHV side. With this calibration factor, the partial pressure of the gas under analysis on the RGA and the partial pressure of the analysis gas on the feed side, the permeability through the film can be determined.

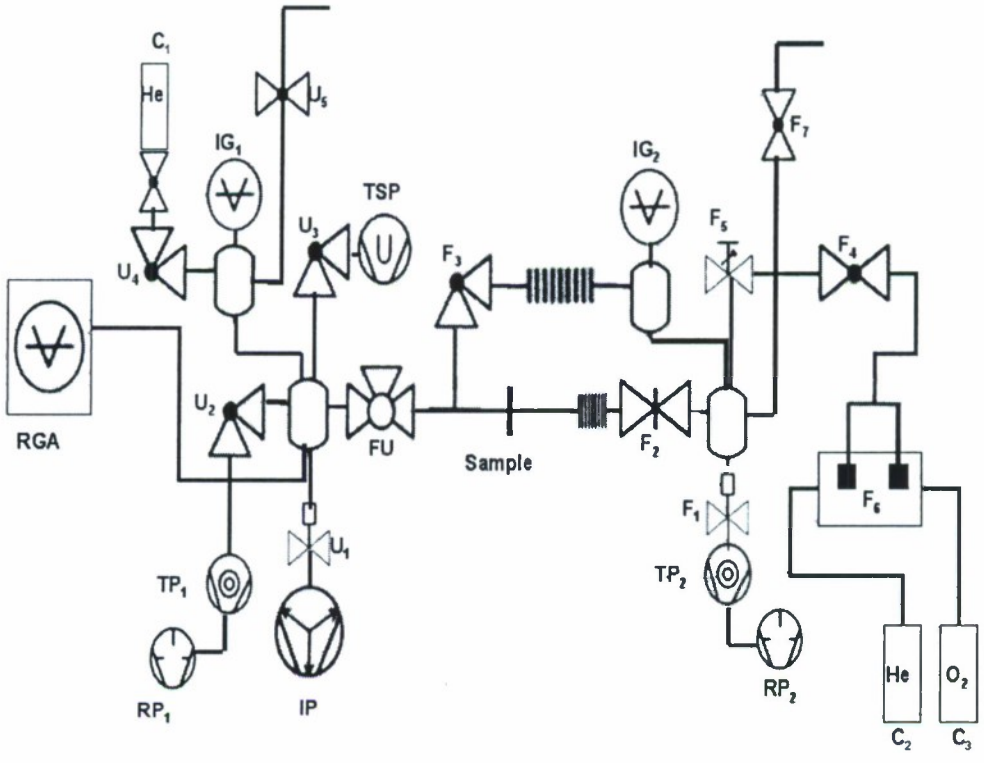

Figure 3.1. Schematic vacuum diagram of the permeation measurement system
RGA: Residual Gas Analyzer, RP: Roughing Pump, TP: Turbo Pump, IG: Ion Gauge, TSP: Titanium Sublimation Pump, FU: Three-position Gate Valve, F_1: Pneumatic gate valve on feed side turbo, F_2: Gate valve on feed side, F_3: Right angle manual bypass valve, F_4: Flow regulator valve on the feed side, F_5: Variable sapphire leak valve, F_6: Gas manifold valves (He and Oxygen), F_7: Vent valve on the feed side, U_1: Pneumatic ion pump gate valve, U_2: Right angle manual valve on the UHV turbo, U_3: Right angle manual valve on the Titanium Sublimation Pump, U_4: Right angle manual valve on the He calibrated leak, U_5: Vent valve on the UHV side, C_1: NIST Calibrated Helium Leak, C_2, C_3: He/O_2 Gas Cylinders.

During the calibration procedure for helium, the titanium sublimation pump is turned off to prevent any pressure fluctuations during the on-off cycle. The UHV side is continuously pumped with the turbo molecular pump. The ion pump is isolated from the chamber with a gate valve. The continuous pumping of the UHV side during calibration is done to provide the same conditions as when the actual permeability measurement of a sample is made, because for low permeability films the permeation measurement may take up to several days.

The following steps were taken to calibrate the system:

I. From the installed calibrated Helium leak, with a given flow rate (2.7×10^{-8}atm cc-day at 23°C or 6.28×10^{11} He atoms/s), a known amount of helium gas is continuously leaked into the UHV side. The helium pressure on the UHV side is monitored with

the RGA. The UHV side is isolated from the feed side during this calibration procedure. It is assumed that the only source of He is the calibrated leak. The helium partial pressure increased from $7x10^{-12}$ Torr to $1.02x10^{-8}$ Torr with the helium leak open. The UHV helium partial pressure of $1.02x10^{-8}$ Torr corresponds to a flow rate of $6.28x10^{11}$ He atoms/sec.

II. In order to calibrate the system for gases other than helium, and to calibrate for helium over a range of flow rates, we have to introduce a known flux of gas atoms into the UHV side of the system. In order to do this, a three-way gate valve with small orifices of known diameter is positioned between the UHV side and the feed side. The three-way gate valve has two gates with orifices of different sizes in them. The smaller orifice is approximately 200μm, as determined by SEM. We also determine the area of the orifice by comparing the diffusion of helium through the orifice, as compared to the helium-calibrated leak. Since the pressure on the UHV side is orders of magnitude lower than the feed side, it is assumed that back effusion is negligible.[56] The rate of effusion through an orifice is given as:[61]

$$\text{Flux, } \Phi \text{ (atoms/sec)} = \frac{\mathrm{P}(\frac{kg}{ms^2}) * \mathrm{A}(m^2)}{\sqrt{2\pi\, \mathrm{m}(kg)\, \mathrm{k}(\frac{m^2 kg}{s^2 K})\, \mathrm{T}(K)}} \qquad (3.1)$$

where, P is the pressure on the feed side, A is the area of the orifice, m is the mass of the gas molecule, k is Boltzmann's constant and T is the temperature. Knowing from Step I, the Helium partial pressure on the UHV side for the given leak rate of $6.28x10^{11}$ He atoms/sec and by determining the He pressure required on the feed side to achieve the same partial pressure of He on the UHV side, the area of the orifice was determined to be $4.2x10^{-4}$ cm^2.

III. Once the size of the orifice is determined, the system can be calibrated for any gas by measuring the partial pressure on the UHV side as a function of the pressure of gas on the high pressure feed side. The partial pressure on the UHV side is measured with a residual gas analyzer and the pressure of the gas on the feed side is measured with an ionization gauge (10^{-8}-10^{-4} Torr) or a capacitance monometer (10^{-3} to 1000 Torr).

For our operating conditions, the calibration factor for Helium is 3.33 x 10^{20} atoms/sec-torr and the calibration curve is shown in Figure 3.2. Using this calibration factor, the permeability measurement rate, in atoms/s, can be determined by multiplying the steady state partial pressure on the UHV side, in Torr, with the calibration factor. This value is then corrected for the area of the sample exposed. Similarly the calibration factor for O_2 was determined to be 1.73 x 10^{20} atoms/sec-torr and the calibration curve for O_2 is shown in figure 3.3. Depending on the gas, thickness of the film, and permeation rate, the experiments are carried out at a pressure between 1-1000 Torr on the feed side. The permeation rate measured is normalized to atmospheric pressure i.e. 760 Torr. The calibration curves in figure 3.2 and figure 3.3 show the linearity of response in partial pressure of the residual gas analyzer on the ultrahigh vacuum side as a function of helium/oxygen atoms introduced into the chamber [calculated as in step II for calibration procedure] through the calibrated orifices positioned in the three-way gate valve between the two chambers. Four sets of readings were taken under similar conditions. For the

helium calibration, the UHV side was pumped with the turbo pump only, with the ion pump valved off and the TSP off. During the oxygen calibration, the UHV side was constantly pumped with the ion pump and the TSP with the turbo pump valved off.
This calibration factor correlates the partial pressure of the test gas on the UHV side with the flow rate of gas atoms from the feed side to the UHV side through the sample film. The flow rate through an orifice is given as:[61]

$$m = \frac{Molecules\_wt.}{Avagadaos\_no.} = \frac{M}{6.022*10^{23}} \text{gms} \tag{3.2}$$

Boltzmann's constant, k=1.380 x10^{-23} J/K = 1.380x 10^{-6} gcm^2/s^{2}K
T @ Room Temperature ≈290K
Pressure on feed side = 1.45x 10^{-6} Torr = 1.93314x10^{-3} barye(cgs)

$$m = \frac{4}{6.022*10^{23}} = 6.6423*10^{-24}\, gm(cgs) \text{ [for He]} \tag{3.3}$$

Putting values in the equation:

$$\text{Rate of Flux, Ø (atoms/sec)} = \frac{\text{Pressure} * Area}{\sqrt{2\pi mkT}} \tag{3.4}$$

$$\Rightarrow 6.28*10^{11} = \frac{(1.933*10^{-3})Area}{\sqrt{2\pi(6.6423*10^{-24})}(1.380*10^{-16})290} \tag{3.5}$$

$$\Rightarrow Area = \frac{(6.28*10^{11})(1.2923*10^{-18})}{1.93314*10^{-3}} = 4.19816*10^{-4}\, cm^2 \tag{3.6}$$

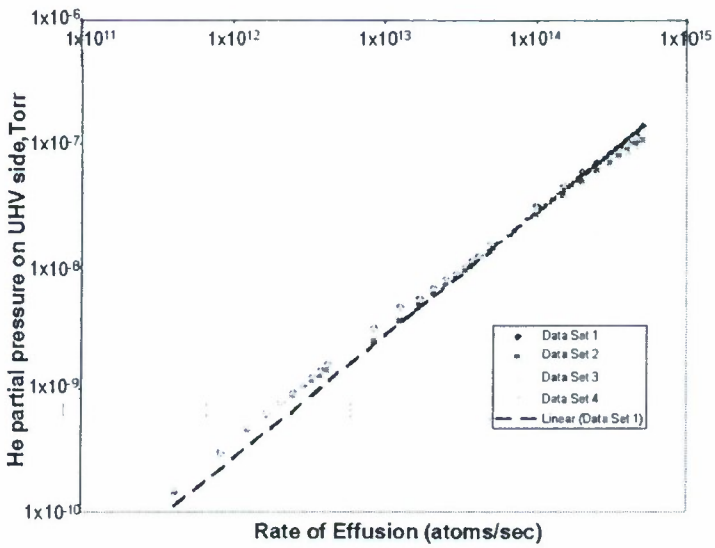

Figure 3.2. Calibration curves for He.

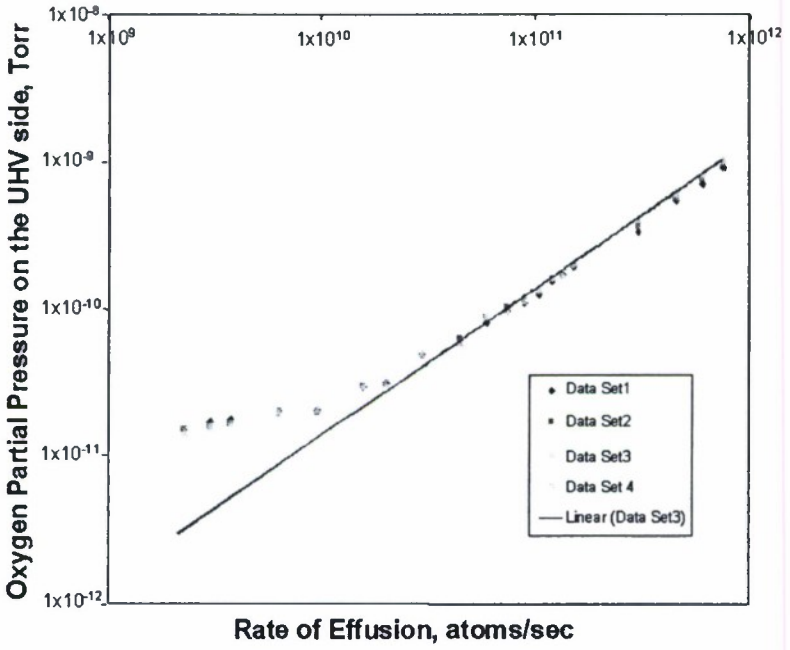

Figure 3.3. Calibration curves for O_2.

The O_2 calibration curve shows that the residual O_2 partial pressure on the UHV side limits the sensitivity to approximately $1x10^{10}$ O_2 molecules / second.

3.1.3 Sample Loading

Loading the sample to be measured is a critical step during the experiment. The requirement for the vacuum seal is that it should not allow analyzing gas to pass around the film from the high-pressure side to the UHV side, nor allow leakage of atmospheric gases from outside the chamber into the UHV chamber. If either case happens, the measured permeability rate will be higher than the actual permeability rate.

The ultrahigh vacuum seal is achieved using an indium wire seal.[56] A schematic cross-sectional view of the arrangement is shown in Figure 3.4. We use two flanges with polished surfaces. The arrangement is polished surface – indium O-ring – sample – indium O-ring – polished surface. During the tightening procedure, care must be taken to not allow the conflat flanges to rotate relative to each other, as it may result in a defect in either the sample or the indium O-rings.

Once the sample is securely held in the sample holder, the holder is mounted in the permeation system. When the sample holder is evacuated, it is important that the pressure on both sides of the sample be reduced simultaneously or else the pressure gradient can damage the sample. For this purpose a bypass valve, F_3, as shown in Figure 3.1, is used.

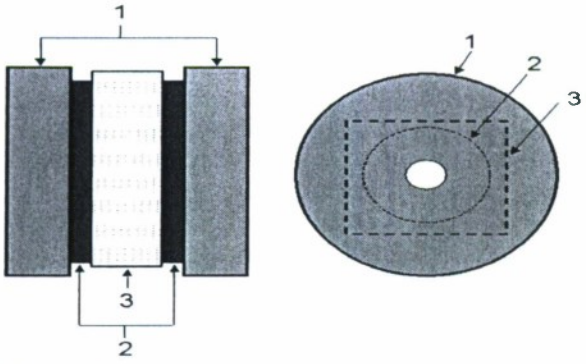

Figure 3.4. Schematic cross-sectional view and side view of the sample arrangement: (1)polished surface – (2)indium O-ring – (3)sample – (2)indium O-ring – (1)polished surface.

3.1.4 Sample measurement

After the sample is securely held in the sample holder, the sample holder is baked at a temperature of approximately 100°C. Only the sample holder is exposed to the atmosphere during the sample loading procedure because the UHV and low vacuum chambers are kept at vacuum during the sample change process. The baking ensures the removal of moisture and helps in lowering the pressure to the desired level.

After the partial pressure of the gas to be studied is reduced to < 10^{-10}Torr, the gas under study is introduced into the high-pressure chamber of the system through the sapphire leak valve. The pressure on the high-pressure side is monitored with a capacitance manometer and is kept constant during the measurement.

The RGA is used to measure the change in partial pressure of the gas under analysis on the UHV side as a function of time. The steady state permeability of the sample is determined once a steady state partial pressure of the gas is reached on the UHV side.

3.2 Barrier Material: Mica

3.2.1 Preparation

The first step required in making barrier layers for attachment to PEN is to have mica layers that are thin enough to provide the required flexibility. Several methods were evaluated to find an efficient way to consistently fabricate thin mica layers from bulk mica.

- The mica surface is hydrophilic and adsorbs water when exposed to a humid environment.[62] The adsorbed water forms layers between the mica layers, assisting the mica layers to slide over one another.[62] In order to introduce water between the mica layers, the bulk material was sonicated in water for one minute before drying in N_2. Marginal improvement in the peeling process was achieved using this procedure. Because of the moisture, the mica layers tended to stick to each other after peeling, making the thin sheets difficult to handle.
- We also tried attaching the bulk mica to the substrate, leaving a thin film of mica attached to the substrate with the bulk of the material being pulled away. To facilitate this process, tape was used and two ways were employed; a) holding the mica tightly on a fixed surface and then peeling the layer with the tape, or b) sandwiching the mica between two pieces of tape and pulling them apart. This method resulted in a thin layer of mica stuck on one piece of tape and the remaining sheet on the other. Layers down to 15μm were separated this way. The major drawback however was the increased number of cracks that appeared in the thin layer and hence this method was discarded.

- An H_2O_2 solution (30% by volume) was used to help weaken the attraction between the layers of mica and thus facilitate the peeling process. The mica pieces (received from H.C. Materials Corp. and S. J. Trader Inc.) were dipped in 30% H_2O_2 solution for 3-4 hours at 60°.[63] After treatment, the samples were washed and dried. Solutions of H_2SO_4 and HF at room temperature for 120 h were also used to exfoliate[64] mica to aid peeling. The sample thickness was measured before and after the treatment and the sample treated with H_2O_2 showed the largest increase in thickness. The effect is explained by the mechanism based on the reactivity of the oxygen formed at the initial moments of peroxide decomposition.[63,64] During the exfoliation process, the hydrogen peroxide molecules penetrate the gaps in the structure of silicate layers.[63] The H_2O_2 molecules exchange with water molecules with evolution of oxygen atoms. These oxygen atoms attack the hydroxyl group between the silicate layers causing a release of hydroxyls and separating of the silicate layers.[63] Along with the concentration of the solution, temperature also plays an important role. Increasing the temperature from 40°C to 60°C increases the swelling and shortens the reaction time. However, above 60°C in a H_2O_2 solution, the mica starts decomposing. The mica was then peeled using a razor blade. Layers with a thickness as low as 3μm, with a surface area on ~50cm^2 (figure 3.5) were achieved.

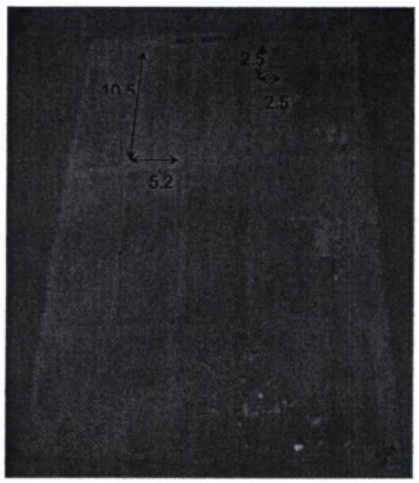

Figure 3.5. Peeled mica layers

3.2.2 Mica-Polymer Stack Formation

Once the mica layers were separated, the next task was to attach them to the polymer substrate. In our experiments, PolyEthylene Naphthalate (PEN) was used as the substrate polymer. Mica layers were stacked with the aim to increase the diffusion path length of gas molecules. The adhesion between the polymer and the mica films plays an important role in the barrier formation. Gaps between the polymer substrate and the mica film resulting because of poor/ incomplete adhesion will provide a pathway for permeating molecules, resulting in a poor barrier. [14] A schematic cross-section of a possible stack is given in Figure 3.6.

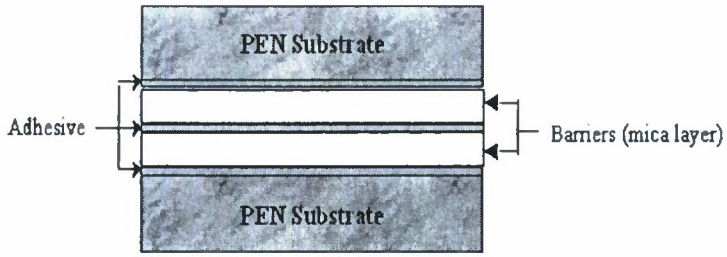

Figure 3.6. Schematic cross-sectional view of a 5"x5" barrier substrate: The PEN substrates are 125μm thick, the adhesive layer is 1μm thick and mica layers are 5-10μm thick.

We tried to make the PEN-Mica-PEN structure using various materials to enhance the adhesion between PEN and mica, as well as exploiting the mica-mica self-adhesion. We also tried double-sided adhesive tape (thickness 10μm), UV curable adhesive and heat-curable adhesive[65] to form a bond between mica and PEN.

- Double-sided tape:
  A thin, 10μm thick, double sided adhesive tape was used for support. The tape was so thin that on removing the backing plastic, it tended to shrink, causing an uneven surface for thin mica layers to stick on. One such stack having four mica layers in between two PEN pieces is shown in figure 3.7 and its transmittance curve is shown in figure 3.8.

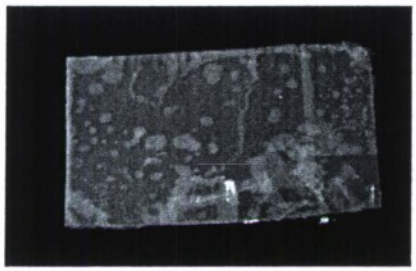

Figure 3.7. Picture of a stack (3"x2") made using double-sided tape– two PEN substrates (125μm thick) sandwich 4 mica films (5μm thick each)

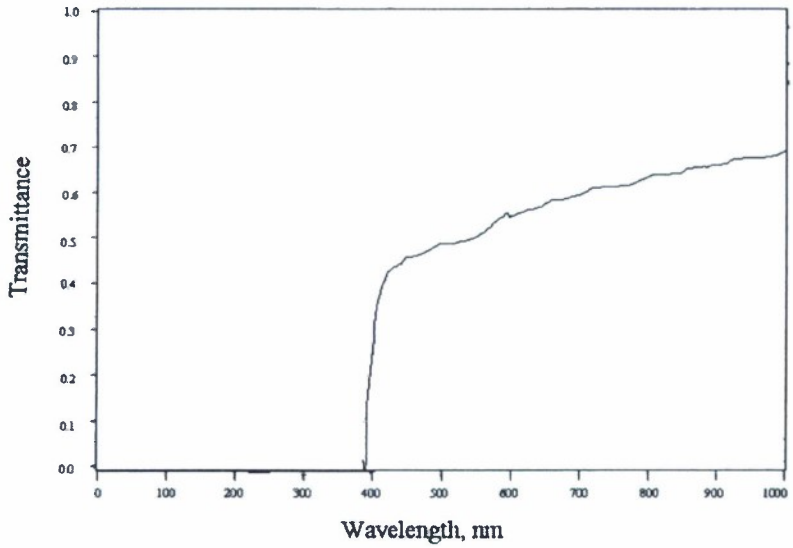

Figure 3.8. Transmittance vs. Wavelength (nm) of the sample shown in Figure 3.7

- UV-Adhesive:
  The advantage in using a UV curable adhesive (Norland Optical Adhesive[66], NOA-72) was that it had a low viscosity (155CPS[66]) and could be thinned even further by adding acetone (up to 20% Volume), without affecting the adhesive properties. The thinner adhesive could be spin coated to give a uniform adhesive layer. Until exposed to UV the adhesive remained a liquid, giving ample time to place the mica pieces in the desired position. NOA 72 is cured by UV light between 315 to 400 nm and visible light between 400 to 450 nm, and after curing has a high transmittance, >90%.[66] This process resulted in many air bubbles trapped between the two surfaces, resulting in very low transmittance, ~60%, as shown in figure 3.10. One of the initial attempts to make a stack using a UV-curable adhesive is shown in Figure 3.9. The stack has four mica layers between two pieces of PEN. We were not able to develop a process where the amount of trapped air bubbles was reduced to an acceptable level.

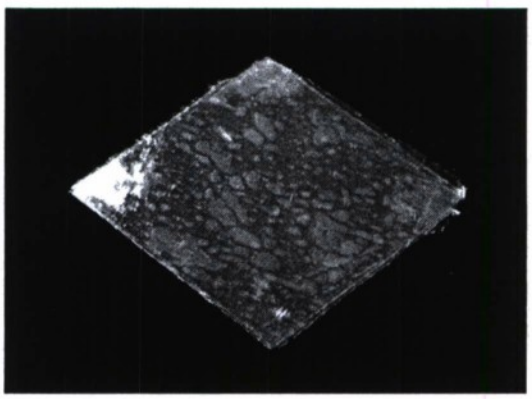

Figure 3.9. Picture of stack (2.5"x2.5") made with UV curable adhesive– two PEN substrates (125μm thick) sandwich 4 mica films (5μm thick each)

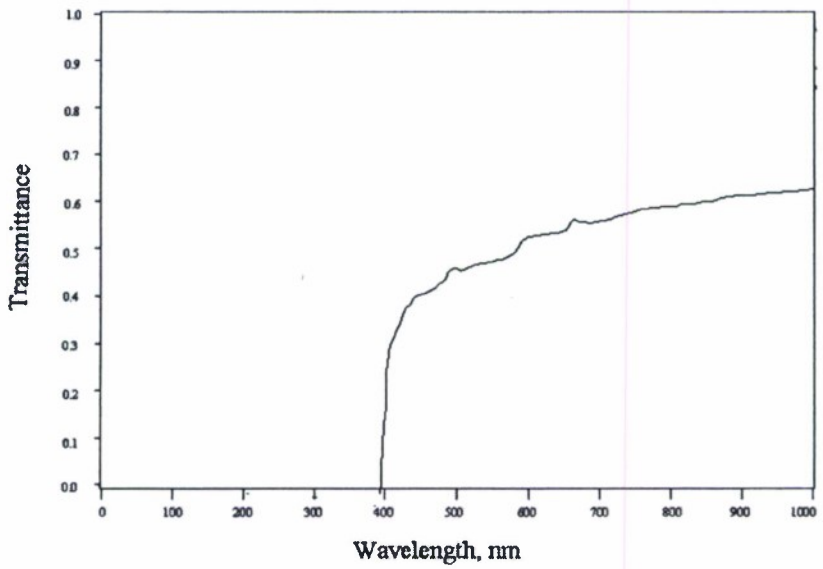

Figure 3.10. Transmittance vs. Wavelength (nm) of the sample shown in Figure 3.9

- Thermal Adhesive:
  Because the UV-curable adhesive did not give an acceptable optical appearance for many applications, we evaluated a heat curable epoxy (Stycast 1266A/B two component epoxy)[67] as the adhesive. This adhesive had a low enough viscosity (650CPS) that it could be spin coated. This epoxy had a setting time of 7 hrs at room temperature and two hours at 60°[67]. This allowed enough time to arrange the mica sheets in the preferred orientation. The advantage of using the thermal epoxy over the UV adhesive was that the thermal epoxy flowed on heating, giving a uniform layer. The improved uniformity provided a higher transmittance, ~ 75%, as shown in Figure 3.11. The heat curable epoxy provides a strong bond between the PEN substrate and the mica layer. A picture of a barrier substrate having four mica layers (5μm) between two pieces of PEN is shown in Figure 3.12.

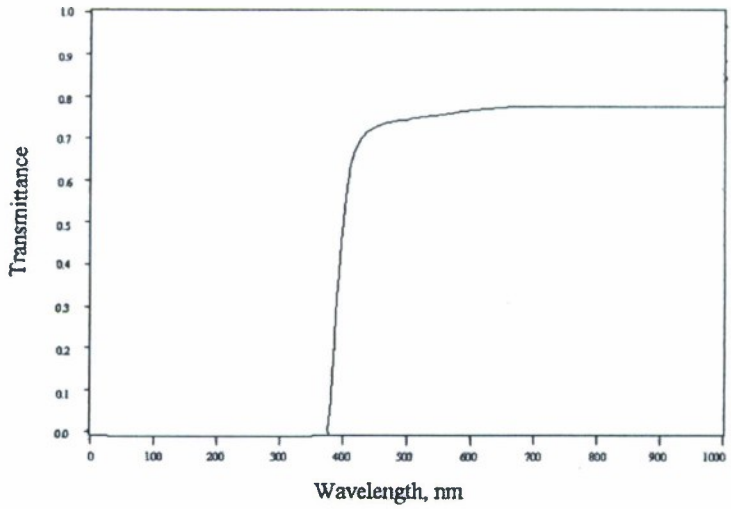

Figure 3.11. Transmittance vs. Wavelength (nm) of sample shown in Figure 3.12

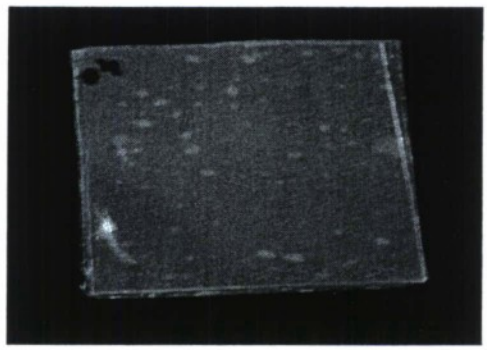

Figure 3.12. Picture of stack (2.5"x2.5") made with thermal epoxy – two PEN substrates (125μm thick) sandwich 4 mica films (5μm thick each)

3.2.3 Transmittance

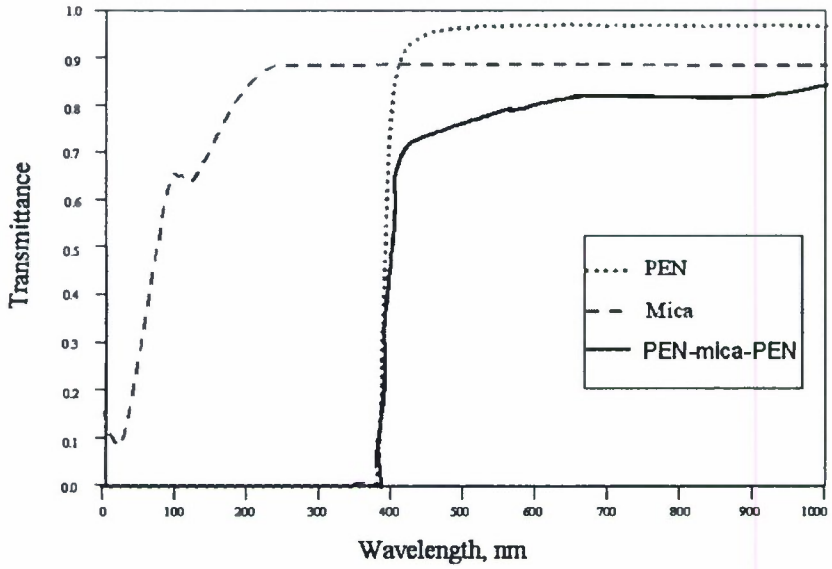

Figure 3.13. Transmittance comparison between a PEN sample (125μm thick), a mica layer (15μm thick) and a PEN- (4 layers of 5μm thick mica)-PEN stack

The polymer substrate, PEN (thickness 125μm) has good transparency (>90%) in the visible range (400nm-650nm). Mica sheet (thickness ~15μm) has a transmittance of ~87% and for a barrier substrate (with four 5μm thick layers of mica between two pieces of PEN), the transmittance is ~75% (figure 3.13).

3.3 Calculations

3.3.1 Calculating permeation rate

After the calibration factor (atoms/sec-torr) is determined, the next step is to calculate the permeation rate through a sample film, given the feed side pressure and the partial pressure of He on the UHV side.

The number of atoms permeating through the sample/sec:

= [UHV Partial pressure reading] x [Calibration factor]

= P_{He} x 3.33 x 10^{20} (atoms/sec)

The above number does not take into account the effects of pressure, P, on the feed side of the system. Normalizing the above value to a standard value @ 760 Torr:

$$= \frac{P_{He} \times 3.33 \times 10^{20} \times 760}{P} \text{(atoms/sec)} \qquad (3.7)$$

The above equation gives the number of atoms permeating through the sample/sec for 760 Torr pressure on the feed side. To get the normalized number for the permeability rate, we need to correct for the area of the sample.

Permeability of He through the sample (area, A = 10.18cm^2 = 1.018x10^{-3} m^2)

$$= \frac{P_{He}(\text{Torr}) \times 3.33 \times 10^{20} (\text{atoms/sec}) \times 760}{P(\text{Torr}) \times A(m^2)} (atoms / \text{sec} - m^2) \qquad (3.8)$$

Converting the permeability rate from atoms/sec-m^2 to g/m^2-day:

$$= \frac{P_{He}(\text{Torr}) \times 3.33 \times 10^{20}(\text{atoms/sec}) \times 760 \times 24(hrs/day) \times 3600(\text{sec}/hr)}{P(Torr) \times A(m^2)}(atoms/day - m^2) \quad (3.9)$$

$$= \frac{P_{He}(\text{Torr}) \times 3.33 \times 10^{20}(\text{atoms/sec}) \times 760 \times 24(hrs/day) \times 3600(\text{sec}/hr) \times 4(g/mol)}{P(Torr) \times A(m^2) \times N_{av}(atoms/mol)}(g/day - m^2)$$

(3.10)

$$= \frac{P_{He}(\text{Torr}) \times 1.43 \times 10^{8}}{P(Torr)}(g/day - m^2) \quad (3.11)$$

where, the molecular mass of He = 4g/mol and N_{av} = 6.022x 10^{23} atoms/mol

3.3.2 Critical Dose Calculations

One of the current theories is that the lifetime of an OLED is limited by how long it takes to oxidize the reactive cathode.[3] A calculation shows that 2 nm of oxide forms on a reactive metal like calcium in 10,000 hours if the permeability rate is 10^{-5} cc/ m^2 per day.[3] The allowable permeation rate is determined to be 10^{-8} g/m^2day for O_2 transmission and 10^{-6} g/m^2/day for water transmission[7] for devices to achieve a lifetime of 10,000 hrs. Thus, the lifetime of the device depends on the number of oxygen/ water molecules reaching the cathode and oxidizing it. Because of the presence of barriers, the cumulative permeation data reaches the steady state regime after an offset time lag. This lag time, before the establishment of equilibrium, could be on the scale of years, suggesting long-lived devices.[48] Hence a better way to report the data would be the time taken to reach the critical dose limit, rather than the steady state permeation rate. In these experiments, the barrier quality is determined by measuring the time taken for a given number of He atoms to permeate through the barrier.

For helium this limit is arbitrarily taken to be

$\Rightarrow 10^{-6}$ g/m^2/day for 10,000 hrs

$\Rightarrow 4.17 \times 10^{-4}$ g/m^2 [in 10,000hrs or 416.67 days]

$\Rightarrow 4.25 \times 10^{-7}$g [through a sample of area 1.02×10^{-3} m^2]

$\Rightarrow 6.4 \times 10^{16}$ atoms

Thus, the critical permeation dose to achieve a lifetime of 10,000 hrs is = 6.4×10^{16} He atoms.

Thus, the critical cumulative dose is 4.25×10^{-7}g of helium passing through the sample barrier substrate. The barrier quality is then described by the time taken to reach this dose. The time taken to reach the critical dose limit (6.4×10^{16} atoms) is determined by numerically integrating the permeation rate as a function of time

The total number of atoms that have passed through the barrier film from the feed side to the UHV side at any time can be given as:

Cummulative Dose (atoms) =[area under the permeation graph]*[Calibration factor]

where the calibration Factor is 3.33×10^{20} atoms/sec-torr for He and the area under the curve is calculated using the area-transform function in Sigma Plot.

3.3.3 Calculating Flexibility of thin Mica layers

One of the key requirements is for the barrier layer to be flexible. Cracking due to mechanical flexing will render the barrier film ineffective. Both the fabrication process and an externally applied bending moment cause strain in the film. Tensile and compressive stresses in the mica barrier layers and shear stress in the adhesive layer have to be considered to determine the level of flexibility of the barrier-substrate.[68]

In our bending test, a rectangular peeled mica film sample, of approximate thickness of ~30μm, was examined under the optical microscope for possible cracks. After bending the mica film around cylinders of different radii, the evolution of crack patterns on the film was monitored using an optical microscope. This bending test was done on several mica sheets of different thicknesses and observed that as the thickness of the sheet decreases, its flexibility increase. Thin mica sheets of thickness ~5μm can be easily bent around a pencil.

When the barrier-substrate stack is bent, the inner surface is in compression while the outer surface experiences a tensile force. A neutral region, where no compressive or tensile strain exists, lies between these two limits.[69] A useful analysis of the mechanics of thin films on flexible substrates has been given by Suo et. al.[69] The governing equations for elastic stresses in multilayered thin films on a thick substrate have been developed by Townsend et. al.[70]

In the case where the barrier film has the same Young's modulus, Y_f, as the substrate, Y_s, the neutral plain is the center of the film-barrier stack, and the strain at the outer surface is given by,[69]

$$\varepsilon_{top} = \frac{(d_f + d_s)}{2R} \tag{3.12}$$

where d_f and d_s are the film and substrate thicknesses, and R is the radius of curvature, as shown in figure 3.14. Assuming that the barrier cracks upon reaching a critical value of strain, it is seen that the minimum allowable radius of curvature scales linearly with the total thickness of the substrate.[69]

When a brittle film is used on a pliable substrate, such that $Y_f >> Y_s$, the neutral plane shifts towards the film, reducing the stress in the top of the film. The resulting film strain is[69]

$$\varepsilon_{top} = \frac{(d_f + d_s)}{2R} \frac{(1 + 2\eta + \chi\eta^2)}{(1+\eta)(1+\chi\eta)} \tag{3.13}$$

where $\eta = d_f/d_s$ and $\chi = Y_f/Y_s$.

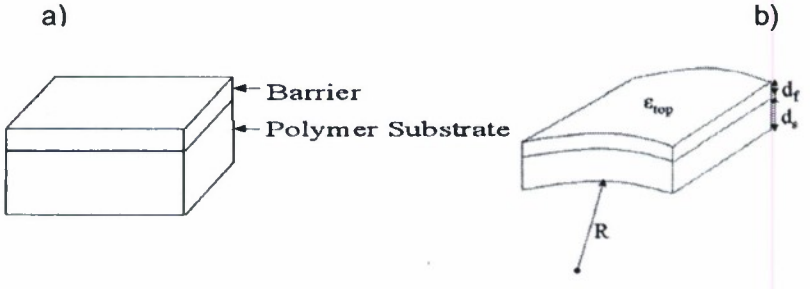

Figure 3.14. a) barrier film-substrate stack b) stack bent around a radius R

The strain in the barrier layer is reduced if it is placed in the neutral surface, sandwiched between two pieces of polymer.[69] Consequently, the bending curvature is no longer limited by

the failure strain of the barrier layer. For a mica sheet, Young's modulus is 25MPa[32] whereas for a PEN substrate Young's modulus is ~6500MPa.[71] The PEN substrate used in our experiments is 125μm thick. The maximum tensile strength for mica is 275MPa[32]. Plugging in the values for d_f, d_s, Y_f, Y_s and maximum allowable strain, ε_{top}=(maximum tensile strength /Young's modulus for mica), into equations 3.13 and 3.12 shows that the PEN-mica structure should be able to be bent around a very small radius.

RESULTS AND DISCUSSIONS

4.1 Permeation results

Permeation rates of helium through bare PEN and PEN-mica$_x$(t)-PEN stacks were measured at room temperature. Helium was used for evaluating the barrier performance of samples using mica thin-film barriers as compared to bare PEN.

Before measuring the permeation of helium through different barrier samples, a test was done on a stainless steel sample (sheet thickness 3mm) to check the sample sealing procedure described in section 3.1.3. The pressure vs. time graph taken from the residual gas analyzer on the UHV side is shown in figure 4.1. After the sample was loaded, the sublimation pump and the ion pump were turned off. For helium permeation measurements, the turbo pump was used to maintain vacuum on the UHV side. The helium partial pressure was approximately 10^{-12} Torr before the measurement started. The feed side was filled with helium gas at a pressure of 760 torr. It was observed that even after > 15 hours, there was no change in the partial pressure of helium on the ultra-high vacuum side. The helium partial pressure on the UHV side was constant at $4x10^{-12}$ Torr. The permeation rate calculated for this partial pressure gives the system a detection limit as low as $5x10^{-7}$ g/m^2-day for helium.

Next a PEN-PEN sample was loaded into the system to determine the permeation rate of He through PEN-PEN. Two pieces of 125μm thick PEN were glued together using thermal adhesive STYCAST.[67] Approximately 1mL of the adhesive was placed on one of the pieces and spun at 1000 rpm for two minutes. The stack was then heated for two hours at a temperature of 70°C, without any application of weight.

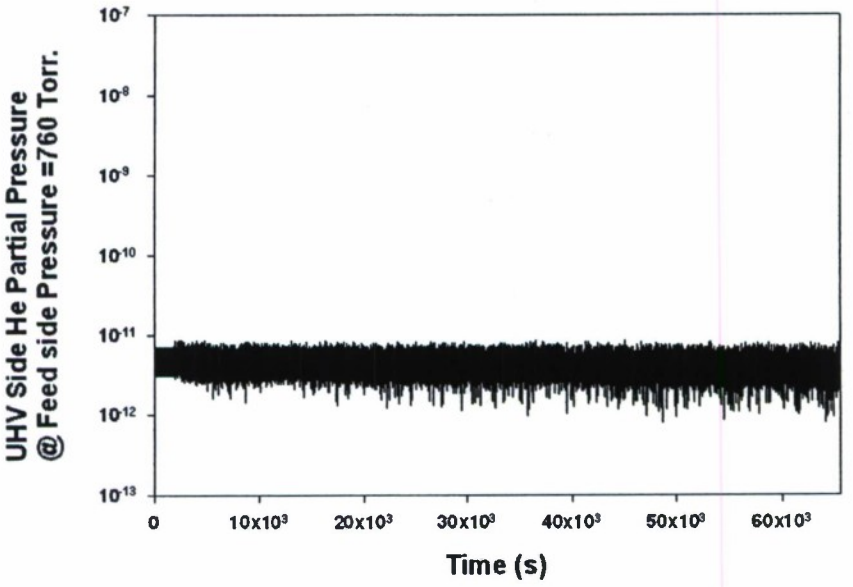

Figure 4.1. The pressure vs. time graph for a stainless steel sample as taken from the RGA on the UHV side. This sets the sensitivity limit for He.

The PEN-PEN sample was measured for He permeation. The rise in the partial pressure of Helium after ~2 hrs of operation seen in figure 4.2 is because of the change in feed side helium pressure from 1 Torr to 1.5 Torr. The change in feed side pressure was made to show

the almost instantaneous increase in helium partial pressure on the UHV side with increase in feed side pressure. The maximum He pressure on the feed side was 1.5 torr. The permeation rate measured at 1.5 torr was then normalized to a value at 760 Torr. The time taken for He gas to permeate through a PEN-PEN sample to reach a steady state was less than 5 min, and the steady state permeation rate, normalized to 760 Torr, was calculated to be 1.73×10^{-2} g/m^2-day as compared to 3.2×10^{-2} g/m^2-day for a single piece of PEN.

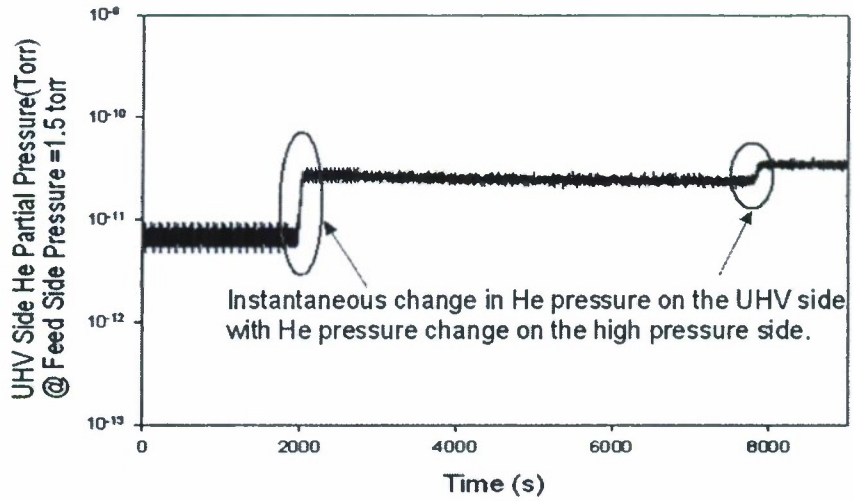

Figure 4.2. The pressure vs. time graph for a PEN-PEN sample showing the instantaneous change in the He pressure on the UHV side with the He pressure change on the high-pressure side (i) from vacuum to 1 Torr (ii) 1 Torr to 1.5 Torr.

While the steady state permeation rate describes the performance of a simple PEN sample, this number does not provide complete information about the behavior of a PEN-mica-PEN sample. A layer of 15μm thick mica was placed between two pieces of 125μm thick PEN using STYCAST[67] thermal adhesive. When the permeation of helium through this PEN-mica-PEN barrier sample was measured with a feed side pressure of ~5 Torr, the steady state permeation rate was found to be 8.16×10^{-3} g/m^2-day. While this value was only approximately 4x lower than that of a bare PEN sample, the time to reach the saturation rate was much longer than for the PEN-PEN sample. As shown in figure 4.2, the change in He pressure on the feed side is reflected within minutes on the UHV side, but for a PEN-mica-PEN sample, the change is more gradual and the time taken to reach the steady state is more than 45 hrs of operation (figure 4.3). A more appropriate assessment of barrier quality is the integrated amount of gas through the sample. We therefore determine the time required for the permeation of mass of a given contaminant, calculated by integrating the area under the permeation curve, as discussed in section 3.3.3.

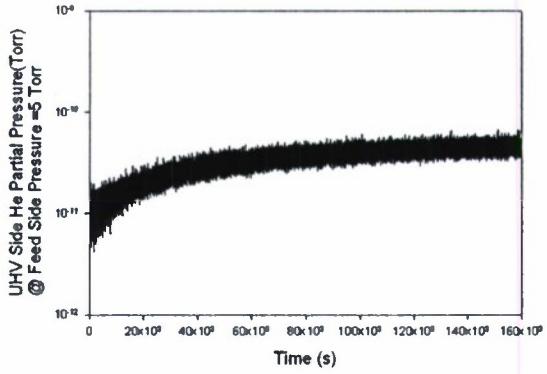

Figure 4.3. Pressure vs. time graph for a PEN-mica(4 films of 5μm)-PEN sample (Feed side Pressure is 5 Torr)

4.1 Effect of mica thickness on Barrier Properties

Different PEN-mica-PEN samples were prepared by placing one mica layer of different thicknesses between two pieces of PEN. The stacks were glued together using thermal epoxy. A plot of the values of the time required to reach the critical dose of 6.4×10^{16} helium atoms as a function of barrier layer thickness is shown in figure 4.4.

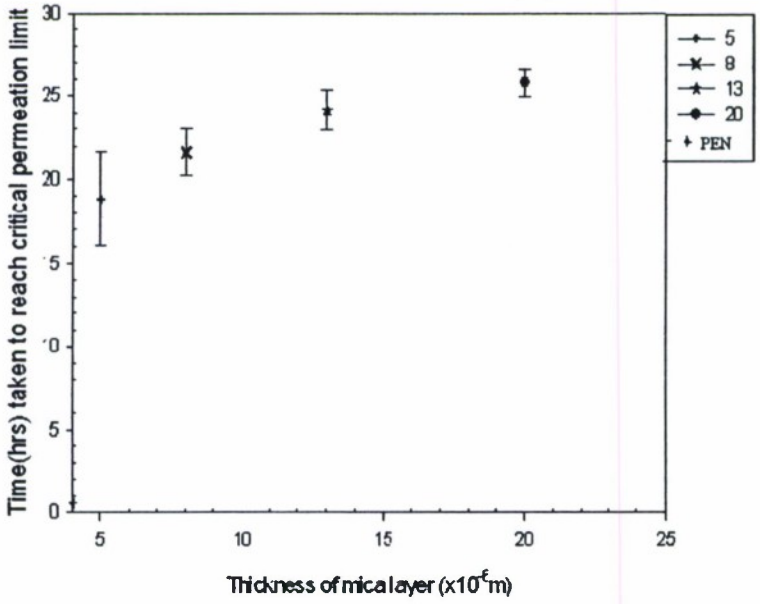

Figure 4.4. Time taken to reach a critical permeation limit as a function of mica thickness sandwiched between two PEN substrates

It is seen that the helium permeation decreases by 30x on adding a thin 5μm thick mica film as compared to bare PEN. Increasing the thickness of the mica layer beyond that causes only small variation in the time taken to reach the critical dose. The time taken to reach the critical dose for a single film of mica of thickness 30μm is ~30 hrs. Thus, adding a single thin mica layer between two pieces of PEN results in a maximum improvement of 45.

Samples were also made with more than one layer of mica sandwiched between two PEN pieces. It was found that having multiple mica layers in the sample had a marginal effect on the time taken to reach the critical dose, as seen in Table 4.1. Thus we can say that the film thickness has a very small effect on the gas barrier properties. Thus, the thinnest mica layer that can be placed within PEN will give barrier properties comparable to thick films. This suggests that the ultimate performance of the mica barrier layer is limited by the number of defects in the mica.

Table 4.1. Comparison of barrier properties for different PEN-mica-PEN samples to show the effect of different number of mica layers in the sample.

Sample Description	Time taken for permeation of 4.25×10^{-7}g of helium (hrs)
PEN-mica(5μm)-PEN	17.25
PEN-mica(10μm)-PEN	21.5
PEN-mica(5μm-5μm)-PEN	22.48
PEN-mica(5μm-5μm-5μm)-PEN	25.20
PEN-mica(5μm- 10μm)-PEN	24.84
PEN-mica(15μm)-PEN	24.12

4.2 Effect of sample bending on Barrier Properties

The time taken to reach the critical dose of 4.25×10^{-7}g of helium by various barrier substrate samples containing mica layers of different thicknesses was measured. These samples were then bent around a cylinder with a diameter of 10 cm, five times in each direction. The permeation properties of the un-bent PEN-mica-PEN samples are compared with that of PEN-PEN sample and the bent PEN-mica-PEN samples in Table 4.2. After bending, the samples had approximately 3x higher permeability as compared to the un-bent sample, but still 8-10x better than bare PEN sample.

Table 4.2. Comparison of Barrier Properties for bent mica-PEN samples.

Sample Description	Steady state Permeation rate for the bent samples (g/m^2day)	Time taken for permeation of 4.25×10^{-7}g of helium (hrs)	
		Un-bent samples	Bent samples
PEN-PEN	1.73×10^{-2}	0.72	0.67
PEN-mica(5 μ m)-PEN	8.10×10^{-3}	17.24	5.80
PEN-mica(10 μ m)-PEN	6.14×10^{-3}	21.50	6.76

These data suggest that defects are generated in the mica layers during the bending process. This is a surprising result, since the mica layer should be in the zero-stress plane in this sample configuration. The defect generation may be due to uneven adhesion between the layers. Also, to compare our experiments with previous work done by others,[13,14,25,26] mica pieces of dimensions around 1x 0.5x 10^{-3} cm were randomly glued between two pieces of PEN to get a net barrier layer of thickness equal to 0.1 cm. Earlier efforts made to incorporate mica into PET films showed a 4-8 times reduction in the permeation levels. The PEN-broken mica-PEN samples took up to 9.7 hrs to reach the critical dose, thus, showing an improvement by a factor of 15, compared to bare PEN.

REFERENCES

[1] J. Lange, Y. Wyser, "Recent Innovations in Barrier Technologies for Plastic Packaging – a Review", Packaging Technology and Science, Vol. 16, pp. 149-158 (2003)

[2] J. Lewis, " Material Challenge for Flexible Organic Devices", Materials Today, Vol. 9, No. 4, pp. 38-44 (2006)

[3] P. E. Burrows, G. L. Graff, M. E. Gross, P. M. Martin, M. K. Shi, M. Hall, E. Mast, C. Bonham, W. Benett, M. B. Sullivan, "Ultra-barrier flexible substrates for flat panel displays", Displays, Vol. 22, No. 2, pp. 65-69 (2001)

[4] Min Yan, Tae Won Kim, Ahmet Gun Erlat, Matthew Pellow, Donald F. Foust, Anil R. Duggal et.al., "A Transparent, High Barrier, and High Heat Substrate for Organic Electronics", Proceedings of the IEEE,Vol.93, No.8, pp.1468-1477 (2005)

[5] S. Forrest, P. Burrows, M. Thompson, " The Dawn of Organic Electronics", IEEE Spectrum, No. 8, pp.29-34 (2000)

[6] J. S. Lewis, S. Grego, E. Vick, D. Temple, "Evaluating and improving mechanical performance of thin films for flexible displays", Proceedings of SPIE, Vol. 5801, pp. 249-260 (2005)

[7] M. E. Gross, G. L. Graff, P. E. Burrows, L.C. Olsen, P. M. Martin, C. C. Bonham and W. D. Bennett, " Ultra-barrier Protective Coatings for Atmospherically Sensitive Thin-Film Electronic Devices", 46th Annual Technical Conference Proceedings, pp. 89-92 (2003)

[8] J. S. Lewis and M. S. Weaver, "Thin-film Permeation Barrier Technology for Flexible Organic Light-Emitting Devices", IEEE Journal of Selected Topics in Quantum Electronics, Vol. 10, No. 1, pp. 45-57 (2004)

[9] M. S. Weaver, L. A. Michalski, K. Rajan, M. A. Rothman, J. A. Silvernail, J. J. Brown, P. E. Burrows, G. L. Graff, M. E. Gross, P. M. Martin, M. Hall, E. Mast, C. Bonha, W. Bennett, M. Zumhoff, "Organic Light-Emitting Devices with Extended operating lifetimes on plastic substrates", Applied Physics Letters, Vol. 81, No. 16, pp. 2929-2931 (2002)

[10] M. D. Groner, S. M. George, R. S. McLean, P. F. Carcia, "Gas Diffusion Barriers on Polymers using Al_2O_3 Atomic Layer Deposition", Apllied Physics Letters, Vol. 88, pp. 051907:1-3 (2006)

[11] N. Inagaki, V. Cech, K. Narushima, Y. Takechi, " Oxygen and water vapor gas barrier poly (ethylene naphthalate) films by deposition of SiO_x plasma polymers from mixture of tetramethoxysilane and oxygen", Journal of Applied Polymer Science, Vol. 104, No. 2, pp. 915-925 (2007)

[12] F.A. Paine, H.Y. Paine, Handbook of Food Packaging, Van Nostrand Reinhold, New York (1992)

[13] E. L. Cussler, C. Yang, "Reactive Barrier Films", Polymers, Laminations and Coatings Conference, No. 3, pp. 1281-1306 (2000)

[14] E. L. Cussler, S. E. Hughes, W. J. III Ward, R. Aris, "Barrier Membranes", Journal of Membrane Science, Vol. 38, No. 2, pp. 161-174 (1988)

[15] P.E. Burrows, G. L. Graff, M. E. Gross, P.M. Martin, M.K. Shi, M. Hall, E. Mast, C. Bonham, W. Bennett, M. B. Sullivan, " Ultra Barrier Flexible Substrates for Flat Panel Displays", Displays, vol.22, pp.65-69 (2001)

[16] G.L. Graff, M. E. Gross, M. Hall, W. Bennett et. al., "Gas Permeation and Lifetime Tests on Polymer-Based Barrier Coatings", Proceedings of SPIE, vol. 4105, pp.75-83 (2001)

[17] D. Feldman, "Polymer Barrier Films", Journal of Polymers and the Environment, Vol. 9, No. 2, pp. 49-55 (2001)

[18] S. Iwamori, Y. Gotoh, K. Moorthi, "Silicon oxide gas barrier films deposited by reactive sputtering", Surface and Coatings, Vol. 166, pp. 24-30 (2003)

[19] E. M. Moser, R. Urech, E. hack, H. Kunzli, E. Muller, "Hydrocarbon Films Inhibit Oxygen Permeation through Plastic Packaging Material", Thin Solid Films, Vol. 317, pp. 388-392 (1998)

[20] B. M. Henry, A. G. Erlat, C. R. M. Grovenor, C. S. Deng, G. A. D. Briggs, T. Miyamoto, N. Noguchi, T. Nijima, Y. Tsukahara, "The Permeation of Water Vapor Through Gas Barrier Films", 44th Annual Technical Conference Proceedings, Society of Vacuum Coaters, pp. 469-475(2001)

[21] F. Dinelli, B. M. Henry, K.-Y. Zhao, A. G. Erlat, C. R. M. Grovenor, G. A. D. Briggs, R. S. Kumar, R. P. Howson, "Characterization of oxide gas barrier films", Proceedings, Annual Technical Conference – Society of Vacuum Coaters, pp. 403-407 (1999)

[22] T. Ohya, M. Yoshimoto, K. Iseki, S. Yokoyama, H. Ishihara, "A Ceramic (SiO_2-Al_2O_3 mixture) Coated Barrier Film by Electron Beam Evaporation", Proceedings, 43rd Annual Technical Conference – Society of Vacuum Coaters, pp. 368-372 (2000)

[23] J. D. Affinito, M. E. Gross, C. A. Coronado, G. L. Graff, E. N. Greenwell, P. M. martin, "A New Method for Fabricating Transparent Barrier Layers", Thin Solid Films, Vol. 290-291, pp. 63-67 (1996)

[24] M. S. Metsik, " Theory of splitting of mica crystals", Soviet Physics(Solid State), Vol.1, No.7, pp.991-997 (1960)

[25] J. Wang, J. P. DeRocher, L. Wu, F. S. Bates, E. L. Cussler, "Barrier Films made with Various Lamellar Block Copolymers", Journal of Membrane Science, Vol. 270, pp. 13-21 (2006)

[26] J. P. DeRocher, B. T. Gettelfinger, J. Wang, E. E. Nuxoll, E. L. Cussler, "Barrier membranes with different sizes of aligned flakes", Journal of Membrane Science, Vol. 254, pp. 21-30 (2005)

[27] http://en.wikipedia.org/wiki/Mica

[28] "Brighter Outlook for mica", Engineering and Mining Journal, Vol. 198, No. 8, p63 (1997)

[29] S. W. Bailey, Paul H. Ribbe et. al., Reviews in Mineralogy, Volume 13: Micas

[30] "Mica". 2007. Encyclopedia Britannica Online: http://concise.britannica.com/ebc/art-2442/The-structure-of-mica-as-exemplified-by-muscovite

[31] Maroo Franzini, "The A and B Layers and the crystal Structure of sheet silicates", Contributions to Mineralogy and Petrology, Vol. 21, pp.203-224 (1969)

[32] D.M. Hepburn, I.J. Kemp, and A.J. Shields, "Mica", IEEE Journal, Vol. 16, No. 5, pp. 19-24 (2000)

[33] L. G. Berry, B. Mason, R. V. Dietrich, Mineralogy: Concepts, Descriptions, Determinations, 2ed., copyright ©1983 by W. H. Freeman and Co.

[34] Y. Hong, N. S. Lennhoff, D. A. Banach, J. Kanicki, "Transparent Flexible Plastic Surfaces for Organic Light-Emitting Devices", Journal of Electronic Materials, Vol. 33, No. 4, pp. 312-320 (2004)

[35] Y. S. Yoon, H. Y. Park, Y. C. Lim, K. G. Choi, G. B. Park, C. j. Lee, D. G. Moon, J. I. Han, Y. B. Kim, S. C. Nam, " Effects of parylene buffer layer on flexible substrate in organic light emitting devices", Thin Solid Films, Vol. 513, No. 1-2, pp. 258-263 (2006)

[36] H. H. Yu, S. j. Hwang, K. C. Hwang, " Preparation and characterization of a novel flexible substrate for OLED", Optics Communications, Vol. 248, pp. 51-57 (2005)

[37] C. Yang, W. H. Smyrl, E. L. Cussler, "Flake alignment in composite coatings", Journal of Material Science, Vol. 231, pp. 1-12 (2004)

[38] D. Perry, W. J. Ward, E. L. Cussler, "Unsteady diffusion in Barrier Membranes", Journal of Membrane Science, Vol. 44, pp.305-311 (1989)

[39] W. J. Ward, G. L. Gaines, M. m. Alger, T. J. Stanley, " Gas barrier improvement using vermiculite and mica in polymer films", Journal of Membrane Science, Vol. 55, pp. 173-180 (1991)

[40] R. K. Bharadwaj, "Modeling the Barrier Properties of Polymer-Layered Silicate Nanocomposites", Macromolecules, Vol. 34, pp. 9189-9192 (2001)

[41] B. Xu, Q. Zheng, Y. Song, Y. Shangguan, "Calculating barrier properties of polymer/clay Nanocomposites: Effects of clay layers", Polymer, Vol. 47, pp. 2904-2910 (2006)

[42] C. Lu, Y.-W. Mai, "Permeability modeling of polymer-layered silicate nanocomposites", Composites Science and Tecjnology, Vol. 67, pp. 2895-2902 (2007)

[43] C. Lu, Y-W Mai, "Influence of Aspect Ratio on Barrier Properties of Polymer-Clay Nanocomposites", Physical Review Letters, Vol. 95, pp. 088303:1-4 (2005)

[44] T. B. Boving, P. Grathwohl, "Tracer diffusion coefficients in sedimentary rocks: correlation to porosity and hydraulic conductivity", Journal of Contaminant Hydrology, Vol. 53, pp.85-100 (2001)

[45] H. T. Rana, R. K. Gupta, H. V. S. GangaRao, L. N. Sridhar, "Measurement of moisture diffusivity through layered-silicate Nanocomposites", AIChE Journal, Vol. 51, No. 12, pp. 3249-3256 (2005)

[46] W. Liu, S. V. Hoa, M. Pugh, "Water uptake of epoxy-clay Nanocomposites: Model development", Composites Science and Technology, Vol. 67, pp. 3308-3315 (2007)

[47] A. Sorrentino, M. Tortora, V. Vittoria, "Diffusion Beavior in Polymer-Clay Nanocomposites", Journal of Polymer Science, Part B: Polymer Physics, Vol. 44, No. 2, pp. 265-274 (2006)

[48] G. L. Graff, R. E. Williford, P. E. Burrows, "Mechanisms of vapor permeation through multilayer barrier films: Lag time versus equilibrium permeation", Journal of Applied Physics, Vol. 96, No. 4, pp. 1840-1849 (2004)

[49] D. R. Paul, W. J. Koros, "Effect of Partially Immobilizing Sorption on Permeability and the Diffusion Time Lag", Journal of Polymer Science: Polymer Physics Edition, Vol. 14, pp. 675-685 (1976)

[50] http://en.wikipedia.org/wiki/Permeation

[51] http://en.wikipedia.org/wiki/Permeation

[52] E.-A. McGonigle, J. J. Liqqat, R. A. Pethrick, S. D. Jenkins, J. H. Daly, D. Hayward, "Permeability of N2, Ar, He, O2 and CO2 through as-extruded amorphous and biaxially oriented polyester films: Dependence on chain mobility", Journal of Polymer Science, Part B: Polymer Physics, Vol. 42, No. 15, pp. 2916-2929 (2004)

[53] A. L. Baner, R. J. Harnandez, K. Jayaraman, J. R. Giacin, "Isostatic and Quasi-Isostatic Methods for Determining the Permeability of Organic Vapors Through Barrier Membranes", Current Technologies in Flexible Packaging- a symposium, St. Charles, IL, pp. 49-62 (1984)

[54] J. Crank and G. S. Park, Diffusion in Polymers, edited by J. Crank and G. S. Park (Academic, New York, 1968).

[55] US Patent References: 5403464Apr, 1995Emery.

[56] A. Ranade, N. A. D'Souza, R. M. Wallace, B. E. Gnade, "High Sensitivity Gas Permeability Measurement System for Thin Plastic Films", Review of Scientific Instruments, vol.76, pp. 013902(1-5) (2005)

[57] G. Nisato, P. C. P. Bouten, P. J. Slikkerveer, W. D. Bennett, G. L. Graff, N. Rutherford, L. Wiese, "Evaluating High Performance Diffusion Barriers: The Calcium Test", SID Conference Record of the International Display Research Conference, pp. 1435-1438 (2001)

[58] R. Paetzold, A. Winnacker, D. Henseler, K. Heuser, "Permeation rate measurements by electrical analysis of calcium corrosion", Review of Scientific Instruments, Vol. 74l., No. 12, pp. 5147-5150 (2003)

[59] http://www.varianinc.com/

[60] http://www.thinksrs.com/downloads/PDFs/Catalog/RGAc.pdf

[61] P. Atkins and J. de Paula, Physical Chemistry, 7th ed. (Freeman, San Francisco, 2001)

[62] P. B. Miranda, L. Xu, Y. R. Shen, "Icelike Water Monolayer Adsorbed on Mica at Room Temperature", Physics Review Latters, vol. 81, n26, pp.5876-5879 (1998)

[63] A. Obut, I. Girgin, " Hydrogen Peroxide Exfoliation of Vermiculite and Phlogopite", Minerals Engineering, vol.15, pp.683-687 (2002)

[64] A. Sh. Gershenkp, L. G. Gerasimova, "Preparation of Flaky Pearly Pigments", Inorganic Materials, vol. 37, pp. 531-534(2001)

[65] http://www.emersoncuming.com

[66] http://www.norlandprod.com/adhesives/noa%2072.html

[67] http://www.emersoncuming.com/other/1266.pdf

[68] Y. Leterrier, C. Fischer, L. Medico, F. Demarco, J. A. E. Manson, P. Bouten, J. DeGoede, J. A. Nairn, "Mechanical Properties of transparent functional thin films for flexible displays", Proceedings, Annual Technical Conference - Society of Vacuum Coaters, pp.169-174 (2003)

[69] Z. Suo, E. Y. Ma, H. Gleskova, S. Wagner, "Mechanics of rollable and foldable film-on-foil electronics", Applied Physics Letters, Vol. 74, N. 8, pp. 1177-1179 (1999)

[70] P. H. Townsend, D. M. Barnett, T. A. Burner, "Elastic relationships in layered composite media with approximation for the case of thin films on a thick substrate", Journal of Applied Physics, Vol. 62, pp. 4438-4444 (1987)

[71] http://www.patentstorm.us/patents/4876137-claims.htm